

## 6 Destructive Testing and Results

Although a large amount of NDE has been performed on CRDMs in the field, very few CRDMs have been tested destructively. Until the study reported here, no through-weld PWSCC in a CRDM had been analyzed destructively, and understanding the crack morphology is important in understanding the NDE responses of this form of cracking. Some techniques, such as ultrasound or deep-penetrating ET, have not been proven effective at finding wastage caused by leaking water.

The destructive examination work is doubly important because the NDE data acquired in the field, at the PNNL round-robin tests, and by the NDE examinations performed by PNNL staff in the laboratory have not conclusively shown where the leak occurred. Although many indications were found in Nozzle 31, the only strong agreement between different techniques occurs at the interface between the J-groove weld and buttering at 200 and 225 degrees. In these locations, ET and PT detected PWSCC-like indications (i.e., tight and meandering).

### 6.1 Cutting Plan

After the NDE results for the two nozzles were examined, it was decided to focus on Nozzle 31. Nozzle 31 was considered to be leaking, and the J-groove weld had several crack-like indications via examinations of replicas of the surface. The first round of cutting was designed to remove the excess carbon steel and Alloy 600 tubing. This cutting served two purposes—it significantly reduced the weight of the sample around the J-groove weld, allowing for easier sample movement, and it created a more favorable geometry for inspection. The cut plan for the weight reduction and tube removal are shown in Figures 6.1 and 6.2.

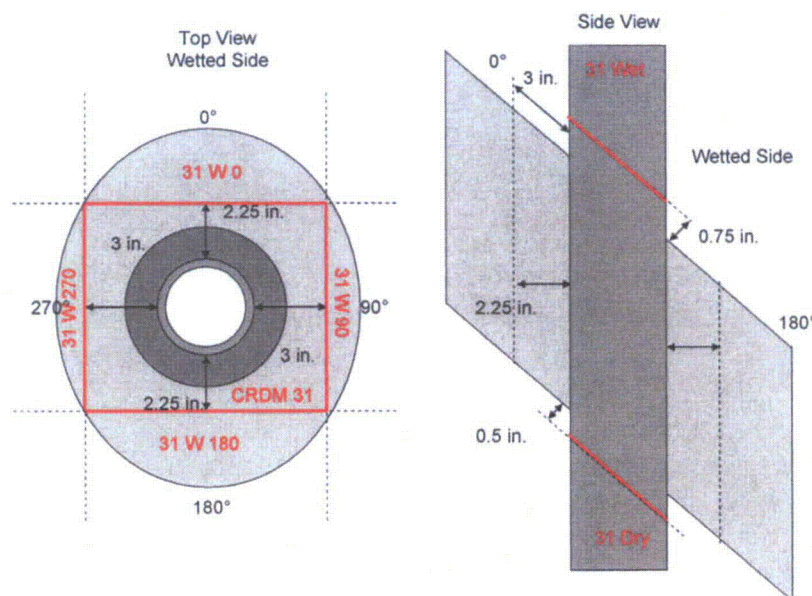
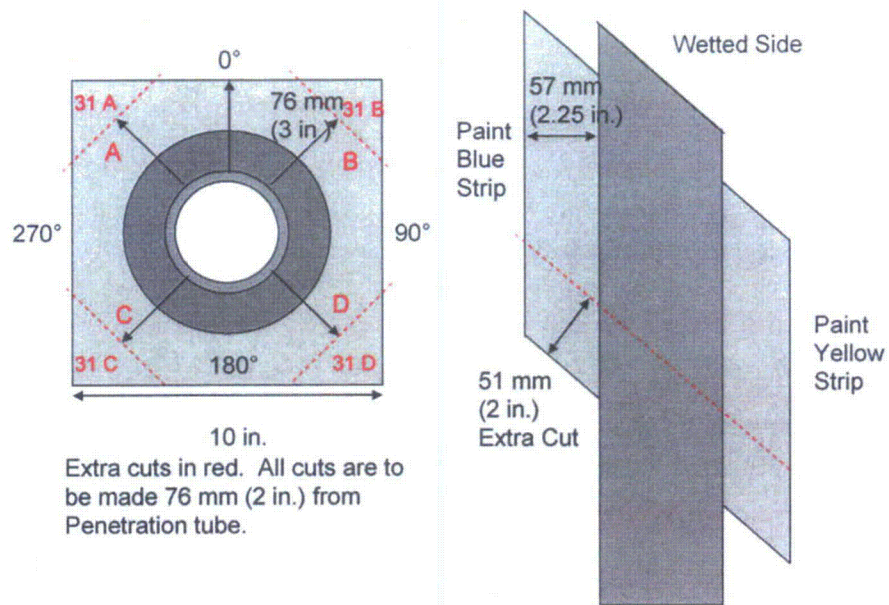
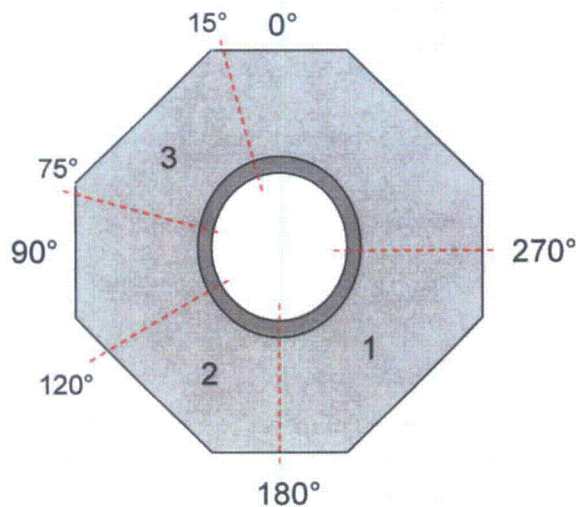


Figure 6.1 Initial Weight-Reduction Cuts Made on Nozzle 31



**Figure 6.2 Additional Reduction Cuts Made on Nozzle 31**

Based on the positive results from ET, VT, and PT, the region from 180 to 270 degrees was considered the most likely to contain a through-wall crack and was designated Section 1. The region from 180 to 120 degrees contained several ET indications and was designated Section 2. The region from 15 to 75 degrees contained a string of small ET indications and was designated Section 3. The section removal plan is shown in Figure 6.3.



**Figure 6.3 Final Cuts Made on Nozzle 31 To Remove Areas of Interest**

## 6.2 Cutting of Nozzle 31

A Marvel Series 8 band saw was used to cut the CRDM. Bimetallic blades were used for the cutting, and the saw and the blades were able to cut with precision through the flame-hardened steel, the 182 weld and buttering, and the Alloy 600 pipe. The saw was installed into a walk-in fume hood for cutting the nozzle. The saw was lifted in by the same crane used to install and manipulate the nozzle. Figure 6.4 shows some images of the saw installation. A contamination containment tent was built around the saw after the saw was installed into the fume hood. While all efforts were made to prevent the spread of contamination inside the tent, the tent provided a physical barrier against the escape of contamination to the uncontrolled areas during cutting and sample movement. The back of the tent was open to the fume hood to allow for constant negative pressure inside the tent. The saw inside the tent is shown in Figure 6.5.

Nozzle 31 was loaded into the tent and cut to remove the extraneous carbon steel not of interest. Figure 6.6 shows the uncut Nozzle 31 on the band saw. Cutting fluid was used to minimize the probability of the cutting creating airborne contamination. The flame-cut regions were difficult to cut through, as the flame cutting had hardened the surface and made it very irregular. In addition, for the first cuts, the sample had to be aligned and held in place using wood blocks and clamps because the nozzle had no flat surfaces.

It was determined that the interior of the penetration tube was the most highly contaminated part of the nozzle. Thus, while the penetration tube did present problems by being in the way of the initial cuts, the ends of the penetration tube were left intact.

Figure 6.6 shows Nozzle 31 after the carbon steel had been cut into a square. After the sample was in this shape, it was much lighter and easy to set securely for cutting.

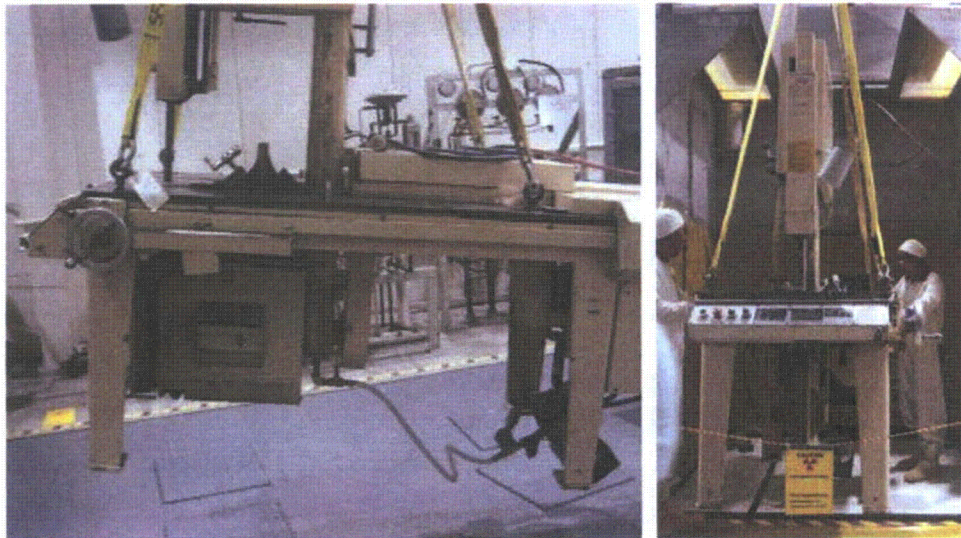


**Figure 6.4 Band Saw Installation into the Liquid Fume Hood**

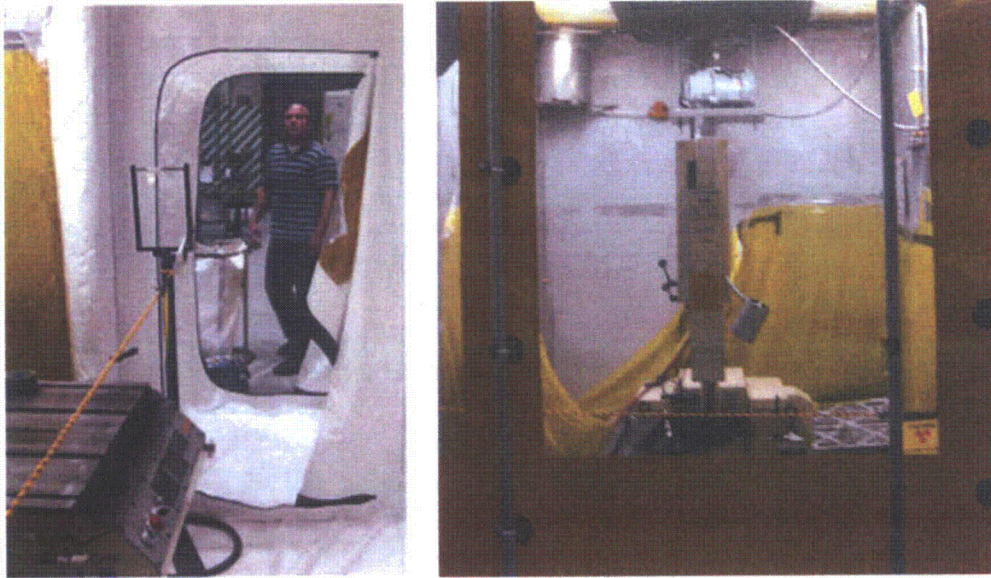


**Figure 6.5 Band Saw Inside Contamination Containment Tent**



**Figure 6.6 Initial Cut on Nozzle 31**

The sample was first cut into a square as shown in Figure 6.7, and then the corners were cut off to form an octagon. Once the carbon steel was cut down, the two ends of the penetration tube were cut off.

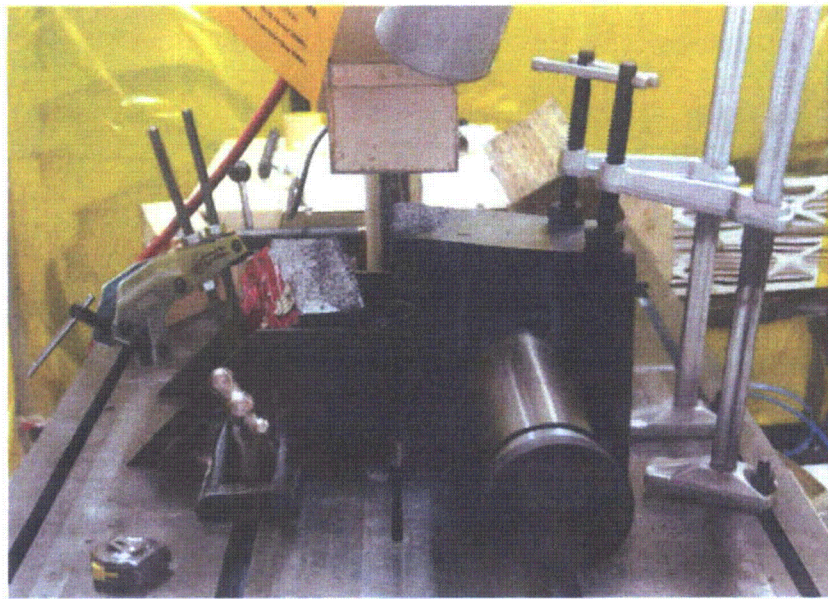


**Figure 6.7 Nozzle 31 After Carbon Steel Was Cut into Square**

To further reduce the weight of the sample and to try to confirm that Nozzle 31 had leaked, 51 mm (2 in.) of steel were cut from the dry side of the nozzle. This slice was then cut in half along the 90- to 270-degree plane and split open, and the 51-mm-long piece of penetration tube was removed. Clear evidence for corrosion was visible on the inside of the interference fit, and a white, crusty buildup was visible at close to 180 degrees.

The next step was to cut away the penetration tube and carbon steel below the J-groove weld. This cutting served two purposes. It reduced the weight of the region of interest, the J-groove weld, and it allowed one to examine the leakage path through the interference fit above the J-groove weld. The excess carbon steel and penetration tube were cut off in two steps, first by removing 51 mm (2 in.) of material from the dry side and then by removing an additional 38 mm (1.5 in.). The areas identified as areas of interest in the cut plan were cut an additional 38 mm (1.5 in.) to just above the triple point of the weld. Each segment of carbon steel was cut in half roughly along the 90- to 270-degree line to release the penetration tube from the interference fit and allow access to the annulus.

### **6.3 Examination of the Interference Fit Region**

The annulus showed clear indications of water flow through the interference fit and the associated boric acid deposits left in the annulus. Two main indications of flow through the annulus were found—a small flow indication at 45 degrees and a very large indication with heavy boric acid deposits ranging from 120 to 190 degrees. A boric acid deposit found from 90 to 120 degrees also is shown in Figure 6.8. Two small flow indications were found close to 200 and 225 degrees. The two main flow indications and the indications near 200 and 225 degrees are shown in Figure 6.9.

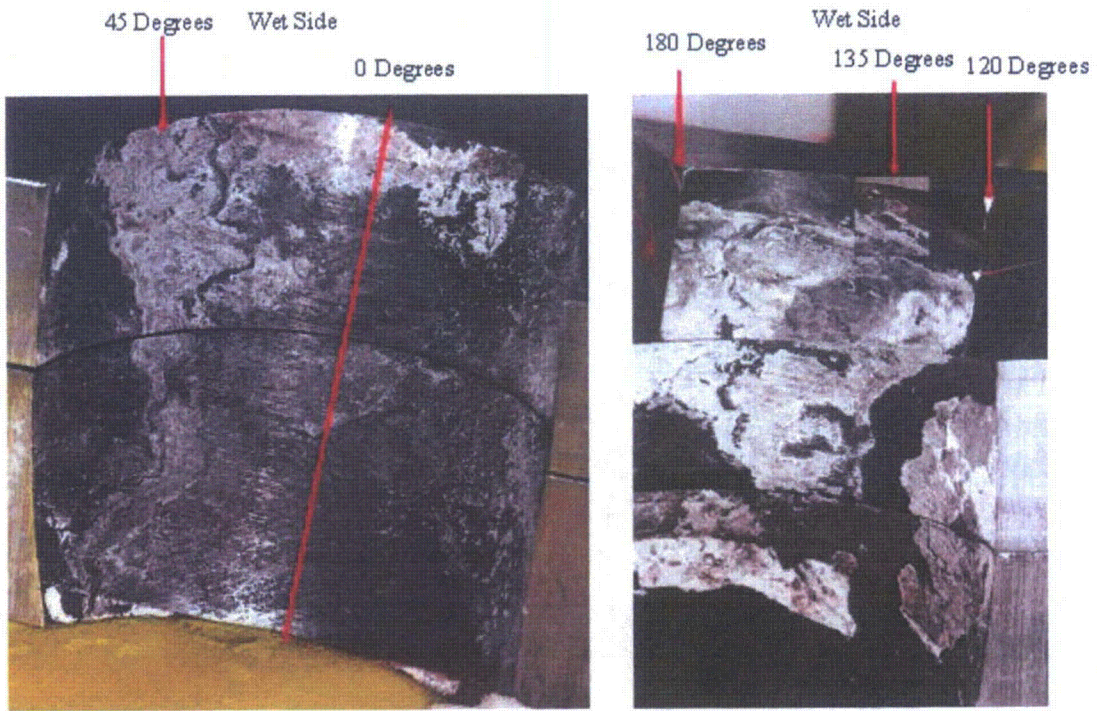


**Figure 6.8 Two Main Flow Regions at 45 Degrees and 120 to 190 Degrees**

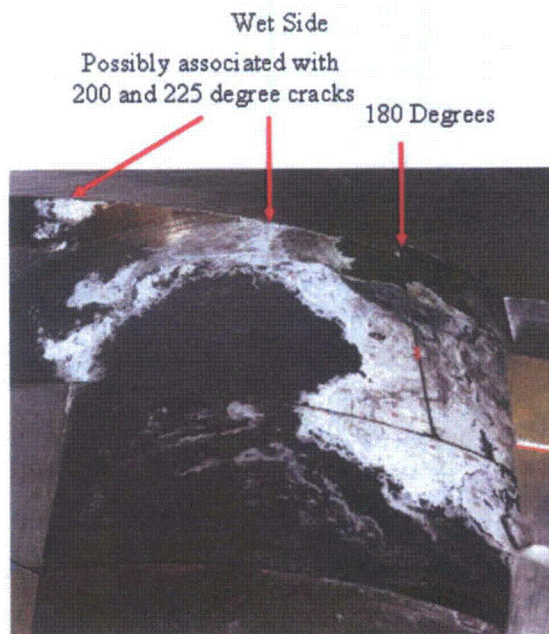


**Figure 6.9 Two Smaller Flow Regions at 45 Degrees and 120 to 190 Degrees**

While the exact depth of the wastage through the interference fit was not measured, it was certainly less than one millimeter, even at the highest flow regions.

## 6.4 Final Sectioning

The three regions identified in the cut plan were cut from Nozzle 31 using the large band saw. These regions were cut from the nozzle after removal of the excess carbon steel. After the sections were cut from the nozzle, the position and extent of the weld, buttering, and triple point were obvious. The pieces were cut just above the triple point to release the penetration tube and allow direct inspection of the buttering above the triple point to determine which of the NDE responses was associated with the through-weld crack. Figure 6.10 shows the three sections after removal from the nozzle, and Figure 6.11 shows Section 2 after further cutting to allow inspection of the buttering.

After the samples were cut above the triple point, the buttering was examined visually and with manual ET. The inspection of the buttering below the triple point would be able to conclusively identify cracks that reached the annulus. The ET scans had to be performed manually because the curved edges and transitions between the buttering and carbon steel produced difficulties in using the *x-y* scanner and extraneous signals at the buttering-steel interface.

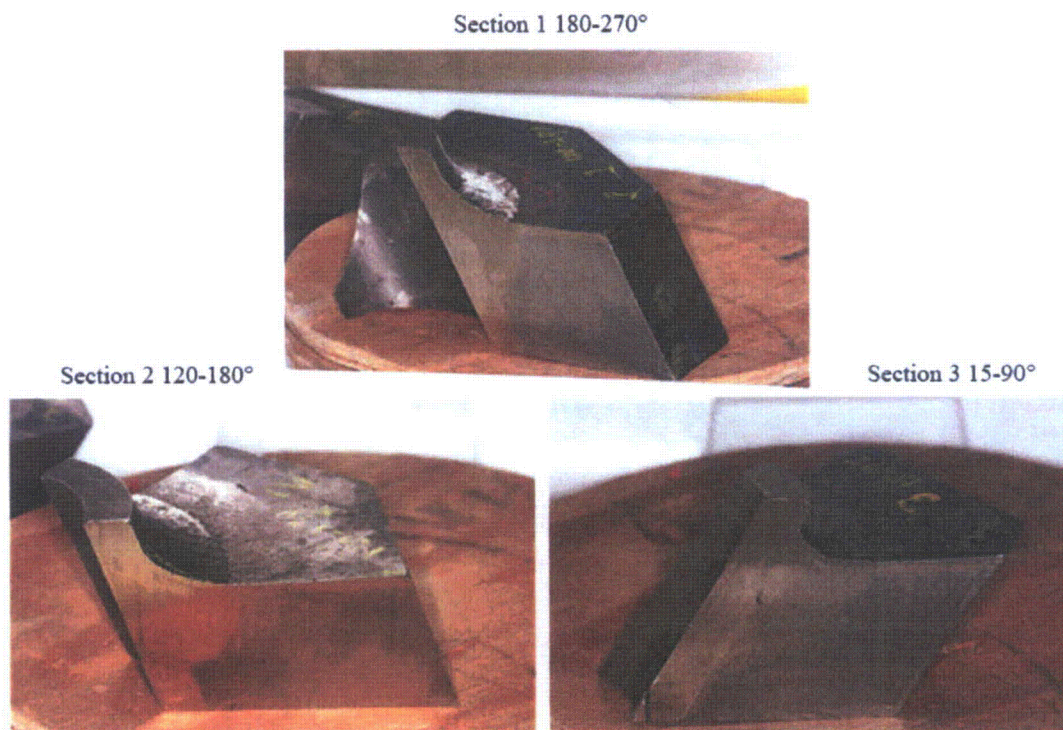
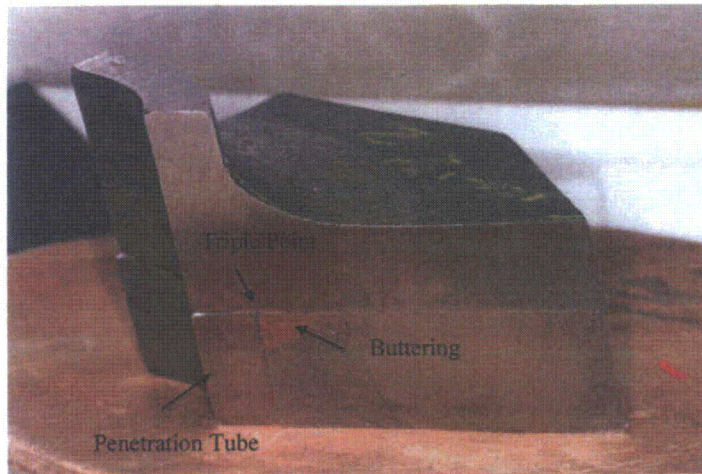
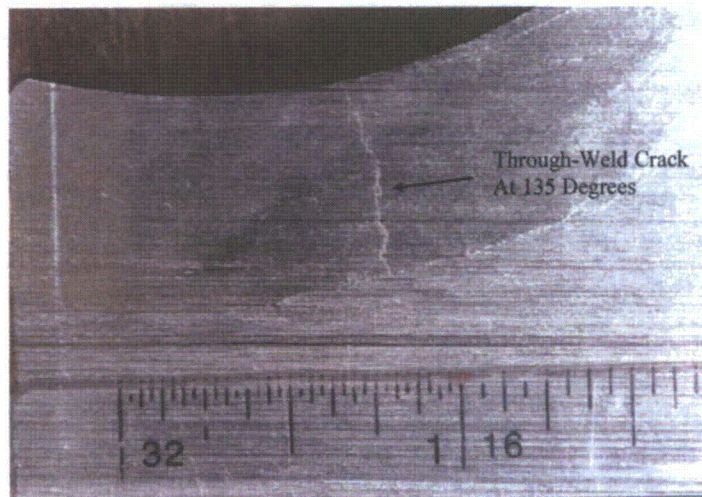


Figure 6.10 Areas of Interest After Sectioning



**Figure 6.11 Section 2 After Cutting Above Triple Point To Remove Penetration Tube**

Careful ET examination and high-resolution photography did not find any evidence of through-weld cracking in Sections 1 and 3. A through-weld crack was immediately apparent, however, in the buttering of Section 2 at 135 degrees. This crack was clearly visible with the naked eye and was confirmed with ET and photography. This crack is shown in Figure 6.12. Because this crack was in a region shown to have crack-like indications and none of the other sections showed any indications of through-weld cracking, all attention was focused on Section 2 near this crack.



**Figure 6.12 Confirmed Through-Weld Crack Found Above the Triple Point in Section 2 at 135 Degrees**

Because five crack-like indications were found by ET centered around 150 degrees, it was not known which crack had propagated through the weld to this point. Additionally, to facilitate destructive testing, the largest piece needed to be less than 16 mm (0.6 in.) thick, so the wetted section was cut into two

pieces 8 mm (0.3 in.) below the wetted surface. Figure 6.13 shows Section 2 after it was cut below the wetted surface.

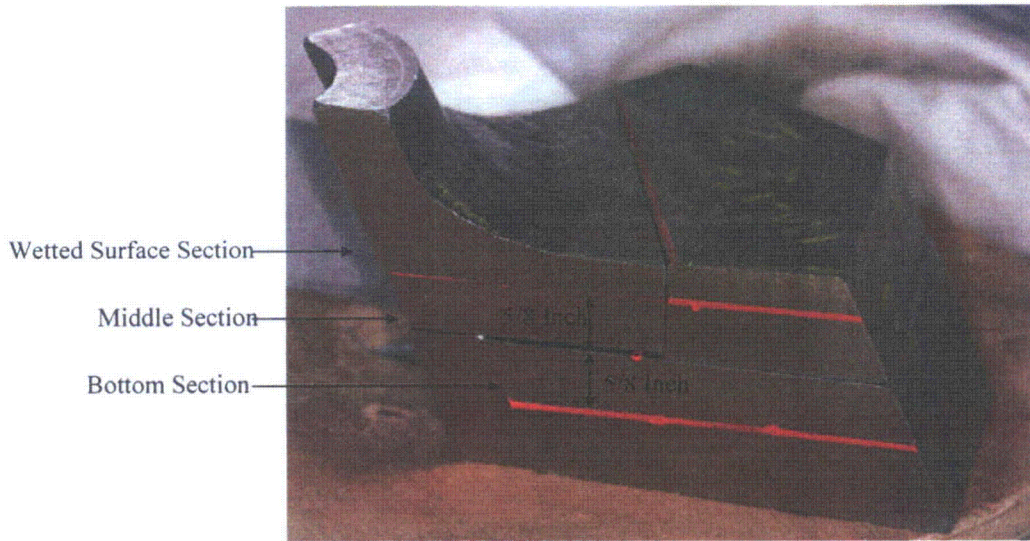


**Figure 6.13 Section 2 After Cutting to Find Cracks**

After the cutting, it was clear, based on the position and spacing of the cracks, which cracks were associated with which ET indications. Figure 6.14 shows the three cracks on the cut face 8 mm below the wetted surface. One interesting aspect of the cracks and the ET indications is how much longer the cracks are 8 mm into the weld than they were at the wetted surface. ET indication 9 is 8 mm long on the surface, and the visible crack length is 21-mm long at the cut surface. ET indication 10 is 6 mm long at the surface and is 25 mm long at the cut surface. Indication 11, which is 10 mm long at the wetted surface, is 15 mm long at the cut surface. The crack spacing is preserved; cracks 10 and 11 are 5 mm apart on both surfaces, and cracks 9 and 10 are 11 mm apart on the wetted surface and 10 mm apart on the cut surface. By contrast, ET indication 8 is 16 mm apart from ET indication 9. It is worth noting that ET indications 8 and 12 do not represent cracks that penetrated 8 mm into the weld.

As final preparation for the destructive evaluation, the cracked sections were cut out in small pieces for easier fine cutting and polishing. The cracked specimens were cut out in five pieces labeled A through E. The cut nozzle Section 2 is shown in Figure 6.15. The through-weld crack associated with ET indication 10 and the nearby crack associated with ET indication 11 are contained in pieces A, C, and E. The nearby crack associated with ET indication 9 is contained in pieces B and D.

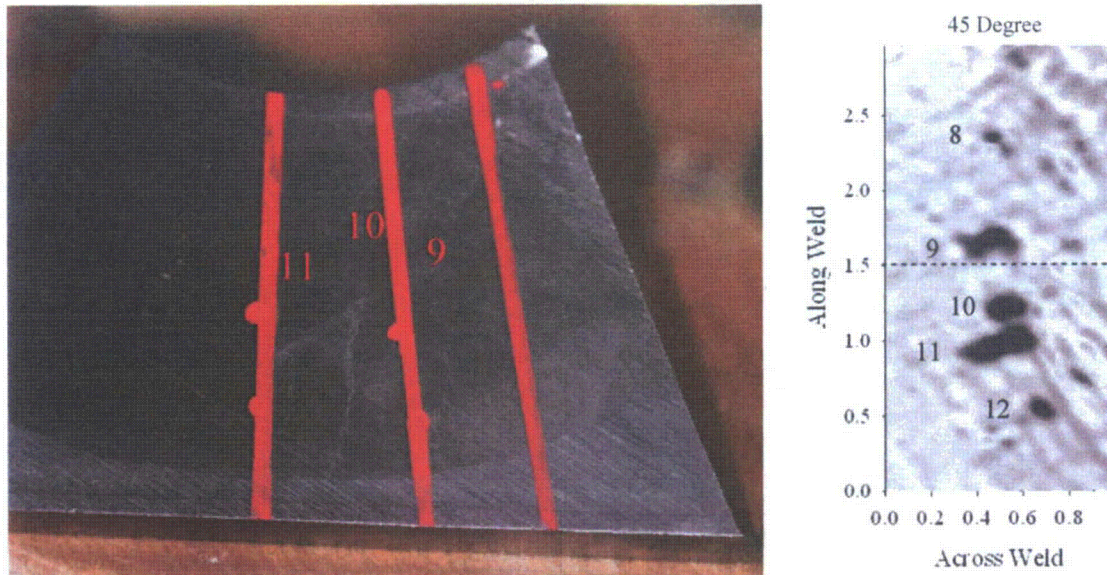


**Figure 6.14 Eddy Current Testing Indications at 145, 155, and 160 Degrees Confirmed Using Destructive Examination**

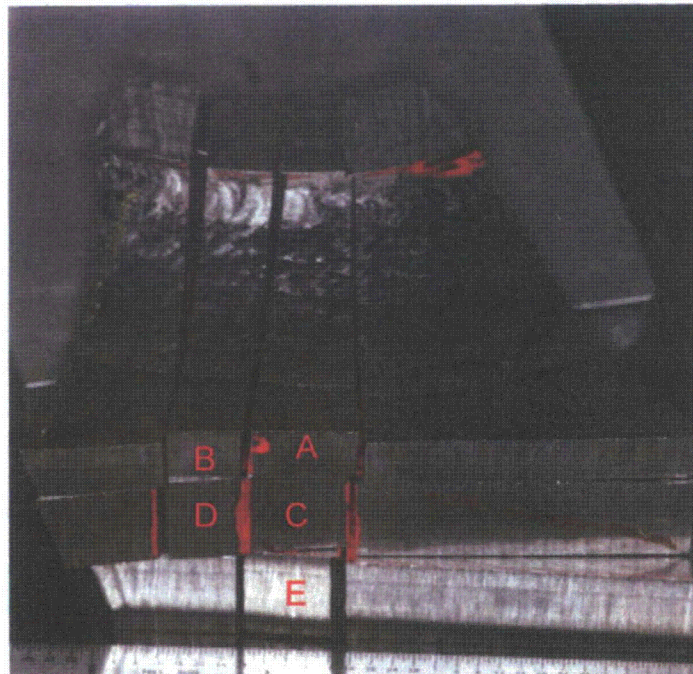


**Figure 6.15 Cracked Metal Coupons Removed from Section 2**

Sections 1 and 3 were then sectioned in a similar way to determine which of the other eddy current indications were associated with deep cracks. Both Sections 1 and 3 were cut 6 mm (0.25 in.) below the wetted surface to find cracks entering the weld metal.

These cuts showed that none of the small ET indications found in Section 1 penetrated 6 mm into the metal. These indications are thus not corroborated by PT, VT, or sectioning. If these indications are associated with cracking, the cracks are relatively shallow.

The 6-mm-deep (0.25-in.) cut in Section 3 found three cracks, at 200, 225, and 255 degrees that penetrated greater than 6 mm (0.25 in.) into the metal. These cracks were further sectioned at 25 mm (1 in.) deep to just beyond the point where the weld ends. It was found that the cracks at 200 and 225 degrees did not penetrate beyond the weld metal, and the crack at 255 degrees penetrated into the buttering past the triple point but did not intersect with the annulus. The crack at 255 degrees penetrated the weld metal and came within a few millimeters of being a leak path but did not break through to the annulus.

## 6.5 Metallographic Examination of Cracking in Nozzle 31 Section 2

Observation of an apparent through-wall crack in Section 2 of Nozzle 31 prompted its further cutting into smaller pieces for destructive examination. Five smaller pieces were received labeled A, B, C, D, and E as shown in Figure 6.15. Pieces A and B are from the inner surface in contact with the PWR primary water, while pieces C and D were from directly above these two sections, respectively. The final piece, E, was from directly above Section C. The positions for pieces A, C, and E are illustrated in Figure 6.16. Pieces A and C contain the Alloy 600 nozzle, Alloy 182 J-groove weld, Alloy 182 butter passes, and low-alloy steel plate. Piece E was above the J-groove weld and was not joined to the Alloy 600 tube. All initial destructive examinations were performed on A, C, and E because they appeared to contain the main through-wall crack. A long secondary crack also was indicated in A that extended into B and D.

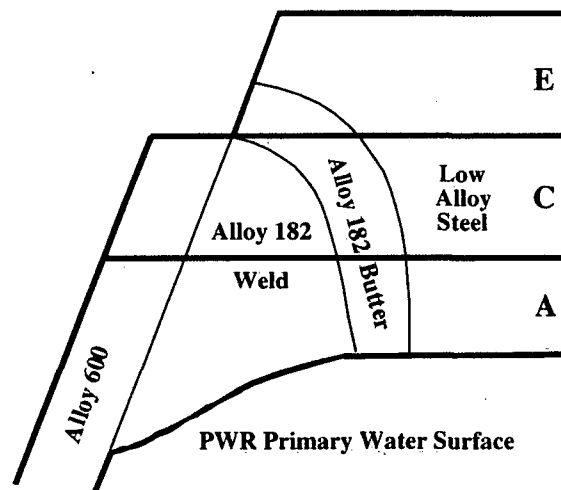


**Figure 6.16** Sections A, C, and E Cut from Section 2 of Nozzle 31. Relative locations are indicated for the Alloy 600 nozzle, the Alloy 182 J-groove weld, the Alloy 182 butter passes, and the low-alloy steel.

### 6.5.1 Initial Examinations and Sectioning

The evaluation of the material began with optical examinations of the top and bottom surfaces of each section using a microscope to identify crack locations and determine serial sectioning locations. Low-magnification photographs are presented in Figures 6.17 and 6.18 for each surface. The dimensions for each piece were somewhat different, with piece A starting at ~8.3 mm (0.32 in.) thick and increasing through the J-groove weld to ~12 mm (0.47 in.) thick, while pieces C and E were ~15 mm (0.59 in.) thick. Careful examinations revealed long cracks on the A, C, and E surfaces, with the longest crack lengths (on A top and C surfaces) reaching ~25 mm (1 in.). The decision was made to limit the required metallography to ten cross sections per piece and maintain a sufficient slice thickness (~2.4 mm (0.1 in.) for subsequent examinations if needed. This resulted in a spacing of ~2.7 mm (0.11 in.) between the metallographic cross sections (blade thickness cut of ~0.3 mm [0.01 in.]) that encompassed the entire crack.

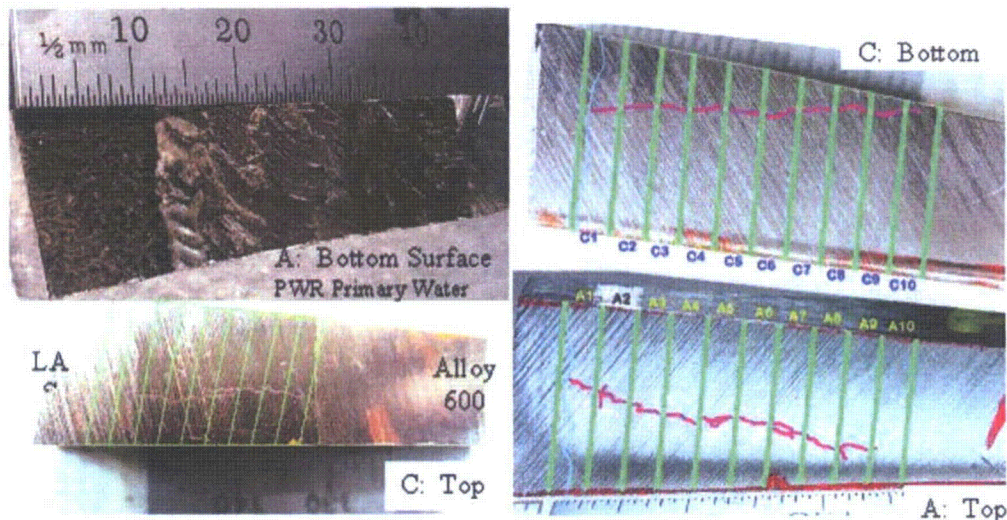


**Figure 6.17** Top and Bottom Surfaces for Pieces A and C with Highlighted Cracks and Proposed Serial Sectioning. The bottom surface for piece A was exposed to primary water during PWR service.



**Figure 6.18** Bottom (left) and Side (right) Surfaces for E with Proposed Serial Sectioning. Note that these images are not to scale with those in Figure 6.17.

The sectioning diagram is illustrated in Figure 6.19 on the same schematic for Section 2 of the Nozzle 31 weldment presented in Figure 6.16. The zero cut was made in the low-alloy steel where no cracking was present, and the remaining cuts were produced parallel to this section. Individual metallographic cross-section samples were identified as A1–A10, C1–C10, and E1–E8. Piece E was shorter than pieces A and C because it was above the J-groove weld and the adjoining Alloy 600 tube detached during initial cutting.

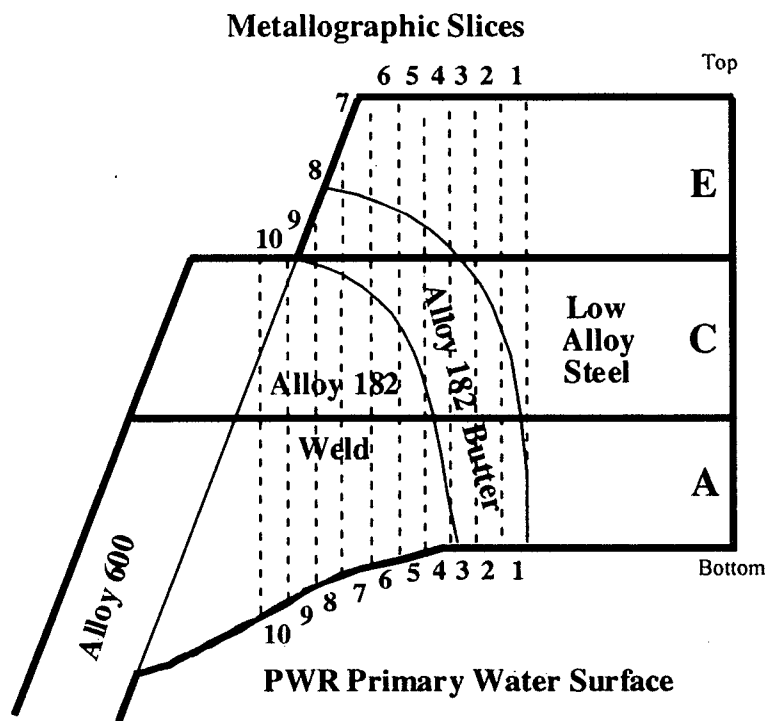


**Figure 6.19** Approximate Locations (dashed lines) of Metallographic Sections Through Pieces A, C, and E

Before the three major pieces A, C, and E were sectioned, additional surface examinations were performed using scanning electron microscopy (SEM) to better document crack characteristics. The A surface exposed to PWR primary water was rough, and relatively thick oxide corrosion products remained in many locations. The SEM images revealed an obvious crack in the Alloy 182 weld metal, perhaps widest in the region near the transition from the butter passes to the J-groove weld metal. A full crack montage is shown in Figure 6.20(a), with a slightly higher-magnification image illustrating the crack morphology in Figure 6.20(b). It is not possible to accurately determine crack openings from these images, but widest locations were on the order of 30  $\mu\text{m}$  (0.0012 in.).

The top (inside) saw-cut surface from piece A enabled a much better observation of the full extent of the cracks. The SEM montages for the two primary cracks observed on this surface are shown in Figure 6.21(a) and (b). The main crack extends to the low-alloy steel interface and well into the Alloy 182 J-groove weld, while the secondary crack is near the edge of piece A and appears to have propagated into the adjacent piece B sample that was not examined. The higher-magnification SEM image in

Figure 6.21(c) documents the tortuous and branched crack path probably along interdendritic and grain boundaries. This will be examined in much more detail on the individual metallographic cross sections.

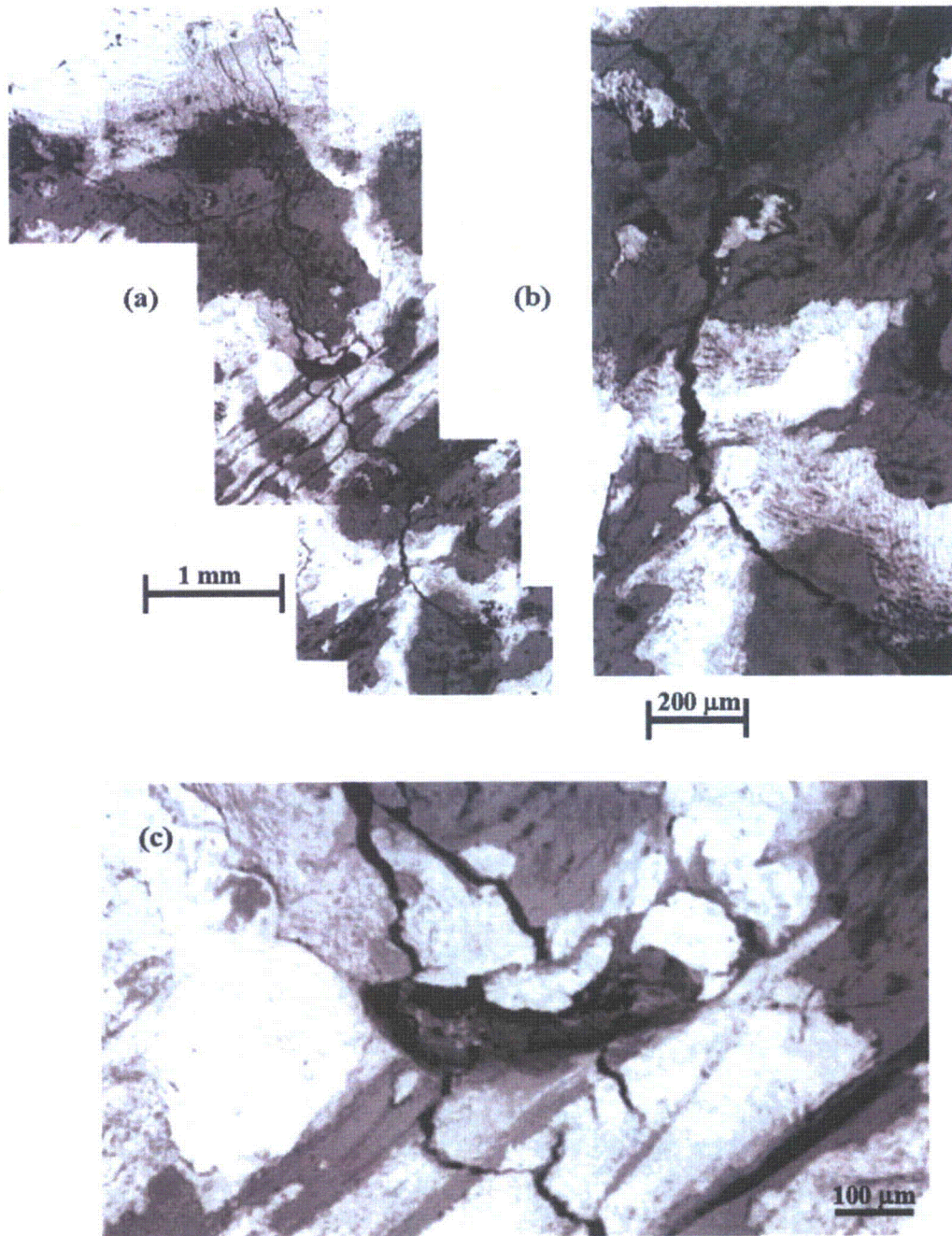


**Figure 6.20** Observed Crack on the PWR Water Surface of Piece A at Two Magnifications. The rough as-welded surface and relatively thick corrosion-product oxide in places (white contrast) made SEM imaging of fine secondary cracks difficult. However, the main crack is seen to extend ~6 mm (0.25 in.) on this surface. A moderate-size defect (pit) near the center of the main crack is shown in (a) and magnified in (c).

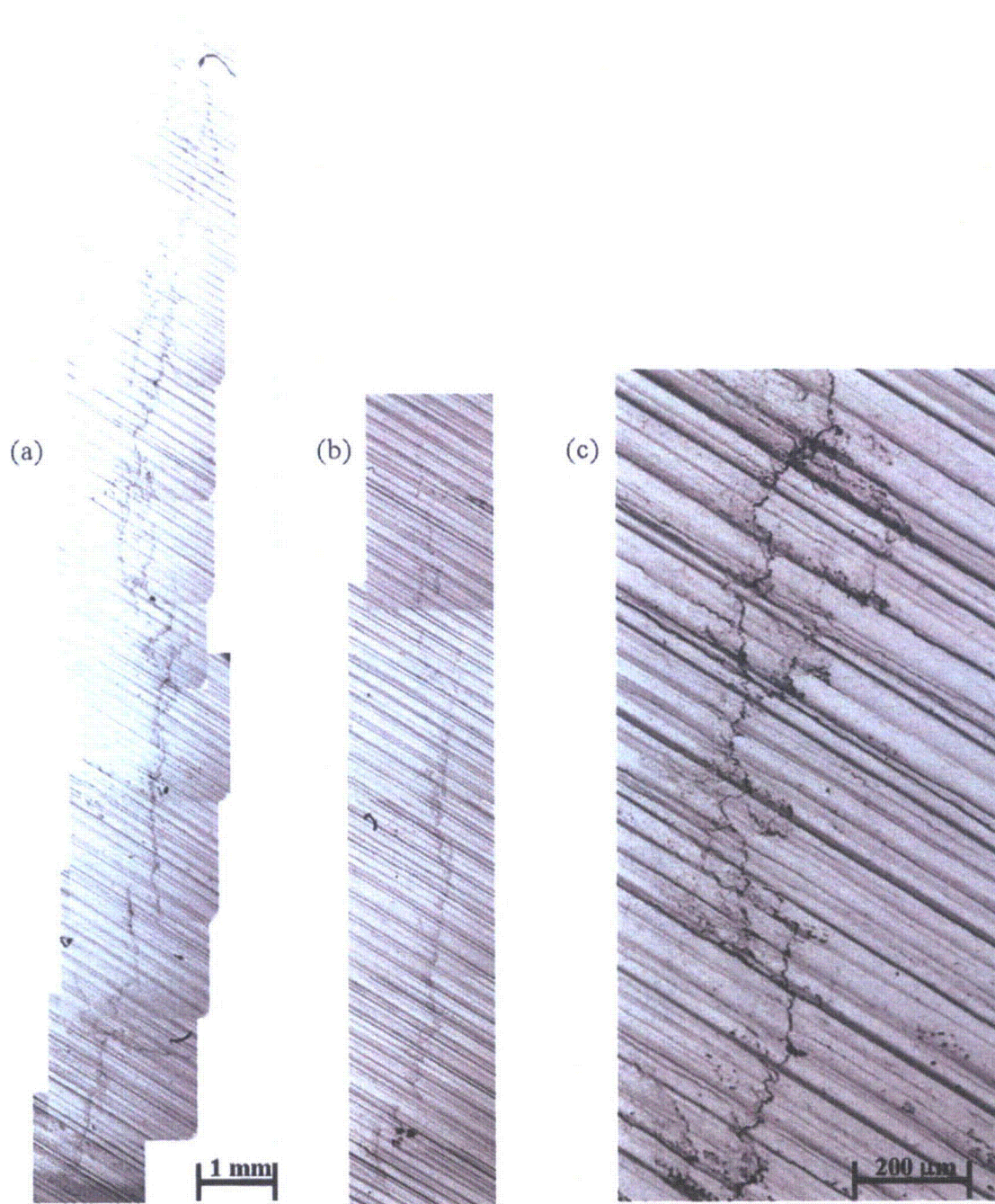


**Figure 6.21 Cracks on Piece A Top (inner) Saw-Cut Surface: (a) main crack, (b) secondary crack, and (c) higher magnification of typical crack morphology from (a)**

The surfaces of pieces C and E also were characterized with SEM before sectioning. The interference-fit gap was identified on the C top surface (facing E) both optically and by SEM, as illustrated in Figure 6.22. In addition to the bottom surface of piece E, the crack exit surface into the gap was examined. The Alloy 182 machined surface that made up the interference-fit gap with the Alloy 600 tube

was found to have two relatively long cracks, as presented in Figure 6.23. When the two cracks were combined, a total crack length approaching ~7 mm (0.27 in.) was found on this exit surface, with the crack opening reaching ~10  $\mu\text{m}$  (0.0004 in.) in places. The cracks were filled with an unknown material, probably boric acid powder and corrosion-product oxide.

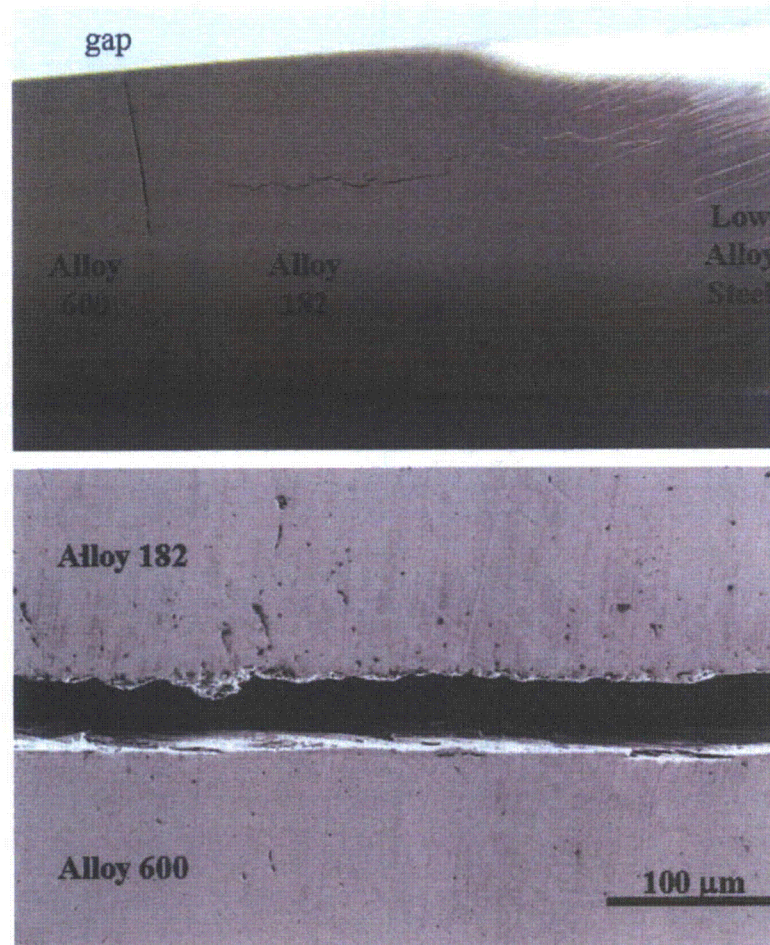


**Figure 6.22 Interference-Fit Gap Between the Alloy 182 Butter Passes and the Alloy 600 Tube on Top Surface of Piece C (facing bottom surface of piece E)**

The pieces A, C, and E were sectioned sequentially, enabling results from initial metallographic examinations on A to help guide sectioning on C and results for C to guide final sectioning of E. Great care was used during low-speed cutting with a diamond saw to maintain cut locations and orientations so that metallographic cross sections from A (A1 to A10) lined up with C (C1 to C10) and that C1 to C8 lined up with E1 to E8. This was done successfully so that the general schematic in Figure 6.19 properly represents locations for all metallographic cross sections.

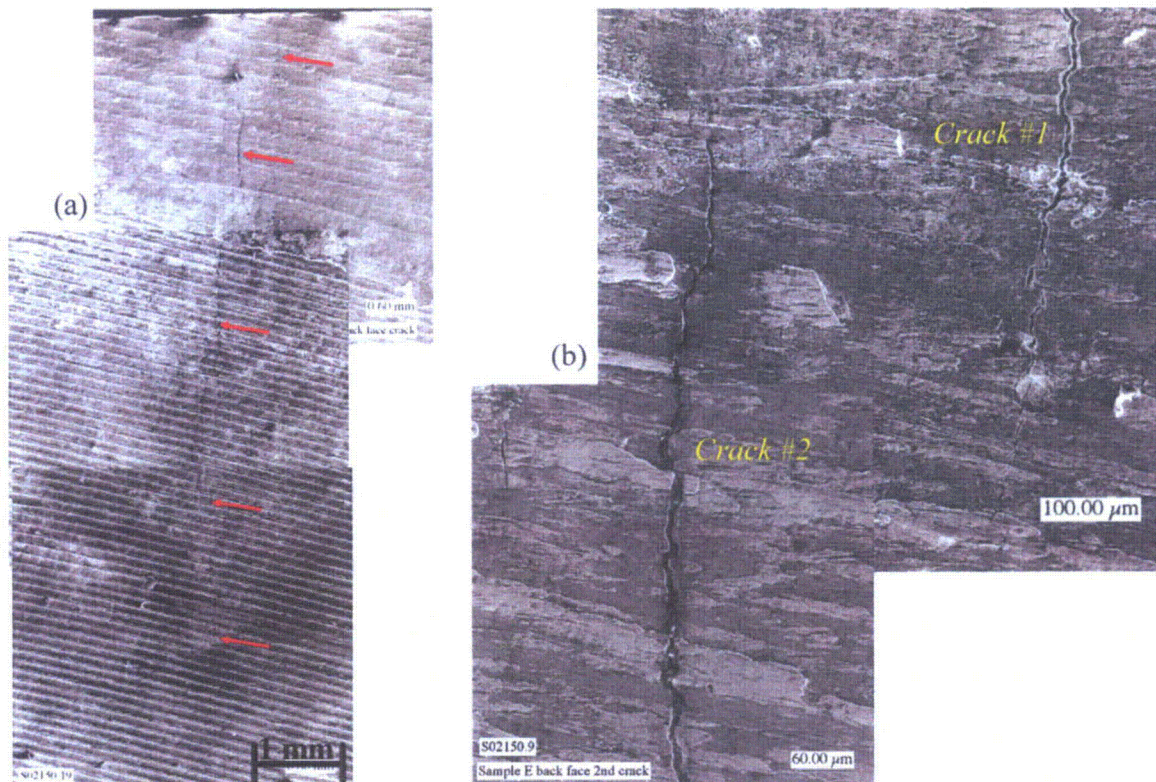


**Figure 6.23 Machined Surface and Exit Location for Through-Wall Cracks from Piece E Alloy 182 Weld Metal into Interference-Fit Gap Between Alloy 182 Butter and Alloy 600 Tube. Low-magnification SEM image (a) shows full length and two major cracks, while higher magnification (b) illustrates crack morphologies.**

### 6.5.2 Metallography of Cross-Section Samples

After pieces A, C, and E were cut, each cross-section sample of interest was placed into a mold to create a liquid acrylic resin mount. Each sample mount was marked to identify the bottom side (toward PWR primary water) and ensure that the proper orientation was maintained throughout preparation and characterization. Samples A0, C0, and E0–E3 were not mounted because no cracks were present so no examinations were needed. The mount and sample measured 19 mm (0.75 in.) in diameter by 12 mm (0.47 in.) in height. Each mounted sample went through a six-step grinding and polishing process using a Buehler Mini Met Polisher to achieve an adequate surface finish for metallography on each cross section. The process started with grinding with diamond-grit lapping pads at 70, 45, and 15  $\mu\text{m}$ . Approximately 15 minutes were required for each of these initial grinding steps with an applied pressure of 2 lb and a speed of 50 rpm. Polishing required another three-step process using Buehler Mastertex or Texmet 1500 cloth and diamond solution for 9-, 3-, and 1- $\mu\text{m}$  finishes. For each step, the appropriate diamond solution was sprayed onto the cloth to polish the samples. Applied pressure and speed used for polishing were identical to those for grinding. Samples were cleaned with distilled water, and the polishing cloth was changed after each step. After the final 1- $\mu\text{m}$  polishing, the cross-section samples were cleaned and dried for optical metallography in the as-polished condition.

Metallographic characterizations included macros of each sample to document the crack location in the cross section, systematic optical metallographs mapping the entire length of primary and secondary cracks, and selected higher-magnification optical images of the area of interest along the cracks. The whole-sample macros consisted of the entire mounted sample to show direction of the crack(s) within each sample. All the images from pieces A, C, and E were oriented the same way in each image, with the wet-side direction at the top of the image to maintain continuity throughout. Examples of the macro images are shown in Figure 6.24 for samples A2, A3, A4, A5, A7, and A9. Cross-section sample A1 was in the low-alloy steel and did not show any cracks, while sample A10 exhibited only a small crack. Sample thickness can be seen to increase moving from the Alloy 182 butter (A2) near the low-alloy steel to the J-groove weld (A4–A9) toward the Alloy 600 tube.

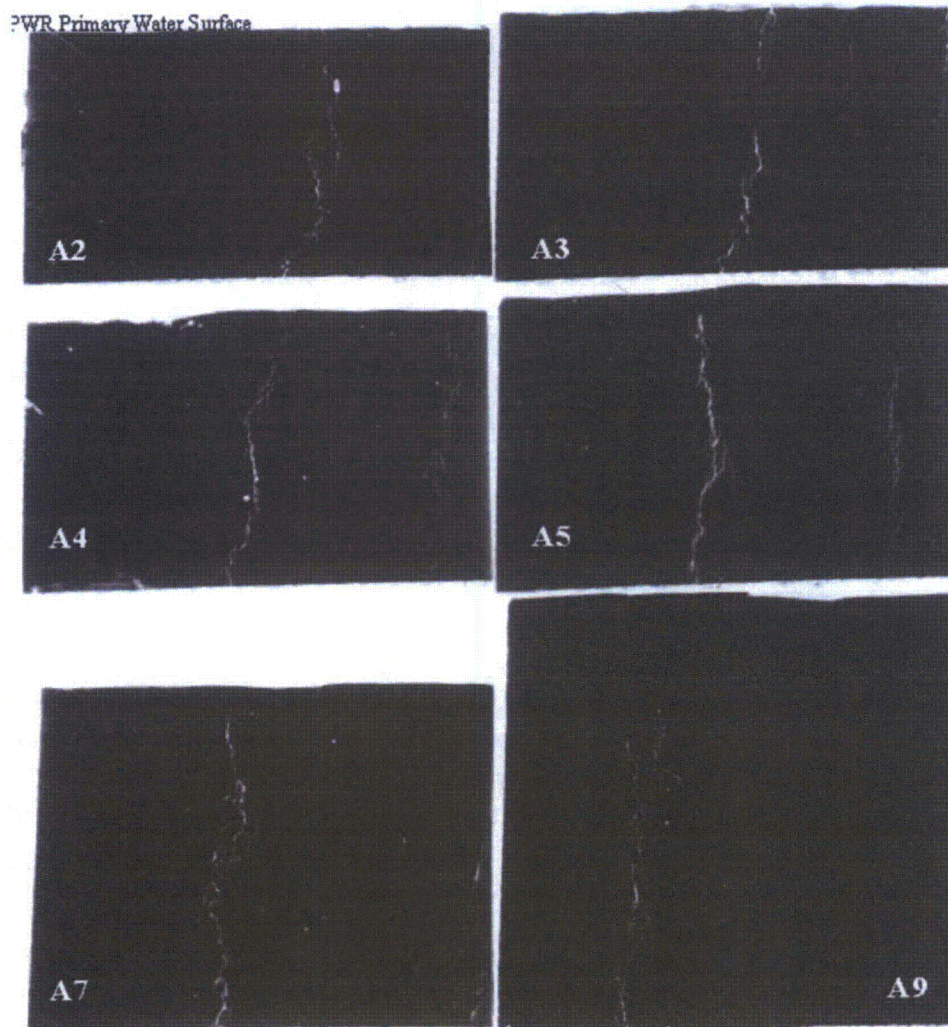


**Figure 6.24** Macro Cracks in Several Cross-Section Samples from Piece A Shown Through Photography. Note that PWR primary water surface is now on the top side of these images.

### 6.5.2.1 Metallography of Piece A Cross Sections

The macro images show extensive cracking through the Alloy 182 weld metal regions with possible initiation sites in cross section A3. A much more detailed evaluation of crack characteristics has been documented by recording systematic images mapping the full range of the cracks in each cross-section sample. Examples of these crack maps are shown for the A cross sections in Figures 6.25, 6.26, and 6.27. The secondary crack present in many of these cross sections also was mapped but will not be presented here. It is sufficient to note that this crack revealed a similar branched morphology.

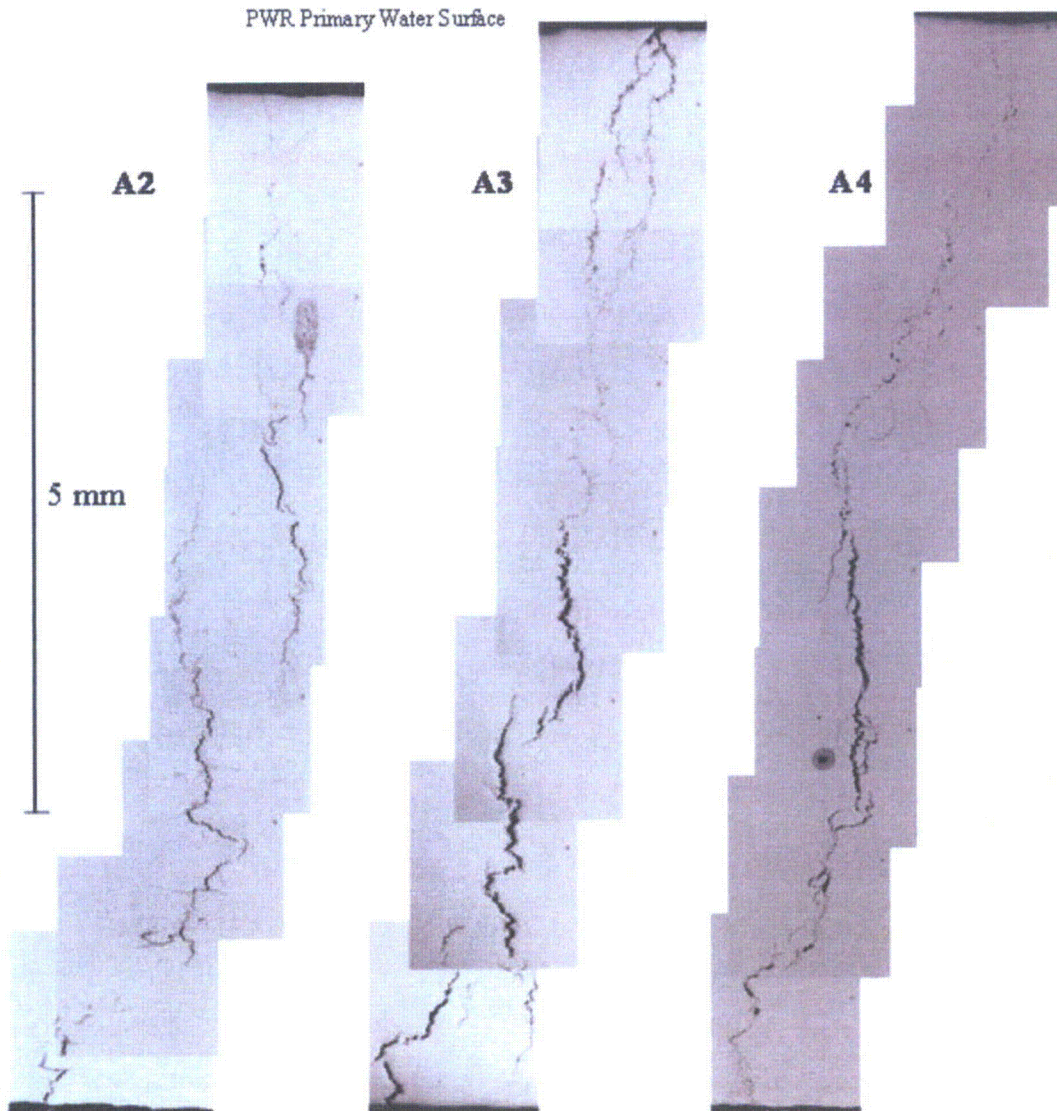


**Figure 6.25 Optical Micrographs for A2, A3, and A4 Cross-Section Samples Showing the Main Crack Essentially Running Through Entire Thickness of Each Sample**

PWR Primary Water Surface

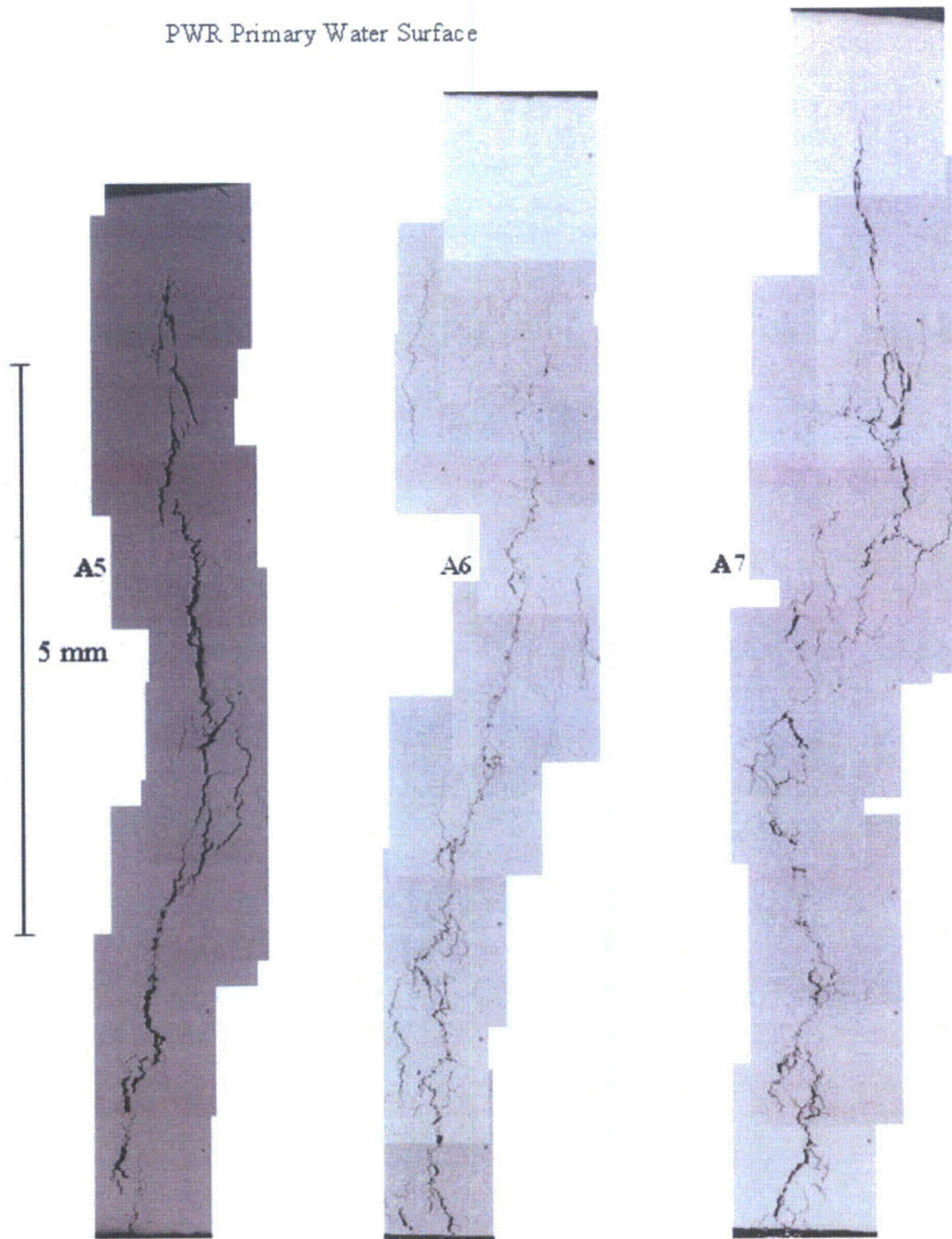


**Figure 6.26** Optical Micrographs for A5, A6, and A7 Cross-Section Samples Showing the Main Crack Appearing Below the PWR Primary Water Surface and Through Remaining Thickness of Each Sample

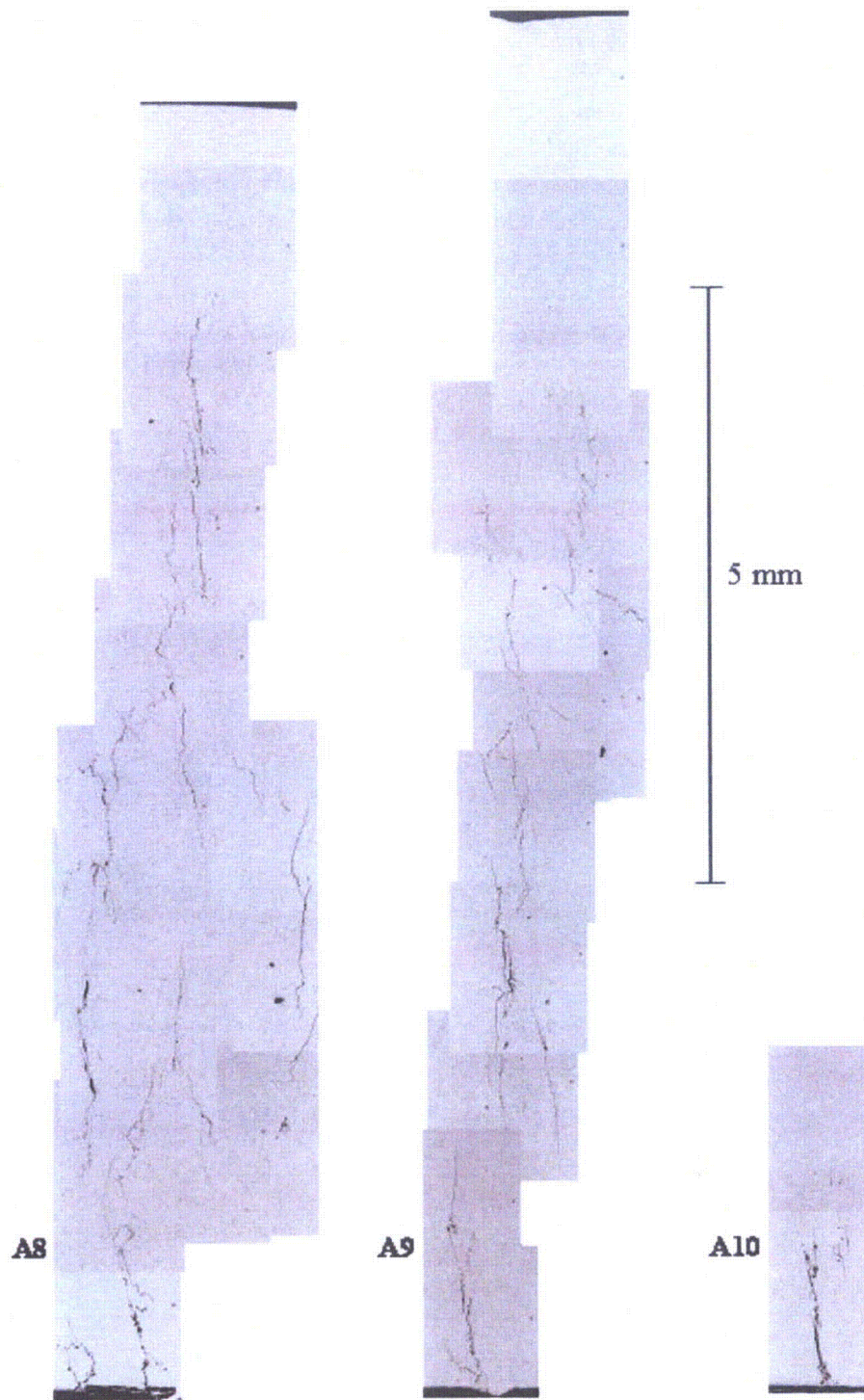


**Figure 6.27** Optical Micrographs for A8, A9, and A10 Cross-Section Samples Showing the Main Crack Appearing Farther Below the PWR Primary Water Surface as a Function of Distance from the Crack Initiation Sites in A3

The apparent crack initiation site is near the A3 slice location, as illustrated in the optical micrograph for this cross section in Figure 6.27 and in a higher-magnification SEM image in Figure 6.28. The SEM micrograph suggests a region of damage at the surface near the crack opening. The width of the crack at the surface in the region is  $\sim 30 \mu\text{m}$  (0.0012 in.), consistent with the SEM examination of the cracks on the piece A primary-water surface presented in Figure 6.20. Crack morphology can be seen as heavily branched immediately below the surface and following convoluted interdendritic or grain boundaries for the most part. The SEM backscatter-electron (BSE) image provides both orientation (grain-to-grain) and compositional contrast. Both can be seen in Figure 6.28, with large grains several hundred micrometers in diameter and finer contrast within grains due to segregation (e.g., manganese and niobium) during final solidification. The heavily branched crack path continues throughout the Alloy 182 weld metal, as illustrated by the tight cracks shown in Figure 6.29. This area is from the mid-depth of the A3 cross section. Similar to the near-surface morphology, the main crack again has split into two separate cracks within this plane and has propagated along parallel interdendritic or grain boundaries. These images from the A3 cross section are representative of the general cracking morphology found within the Alloy 182 weld metal microstructures in nearly all metallographic sections examined.

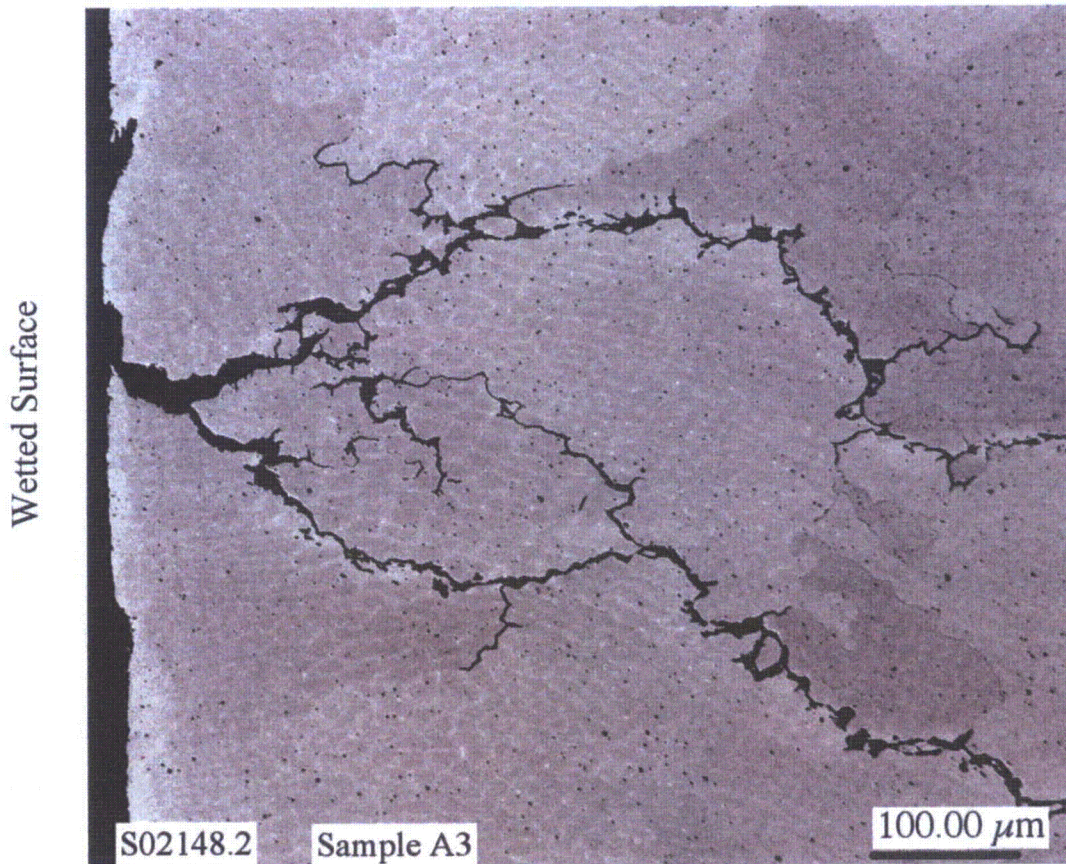


**Figure 6.28** Location Where Crack Intersects the PWR Primary-Water Surface in Sample A3 and May Be Near the Initiation Site. Microstructural contrast within individual grains is due to solidification segregation in the Alloy 182 weld metal.

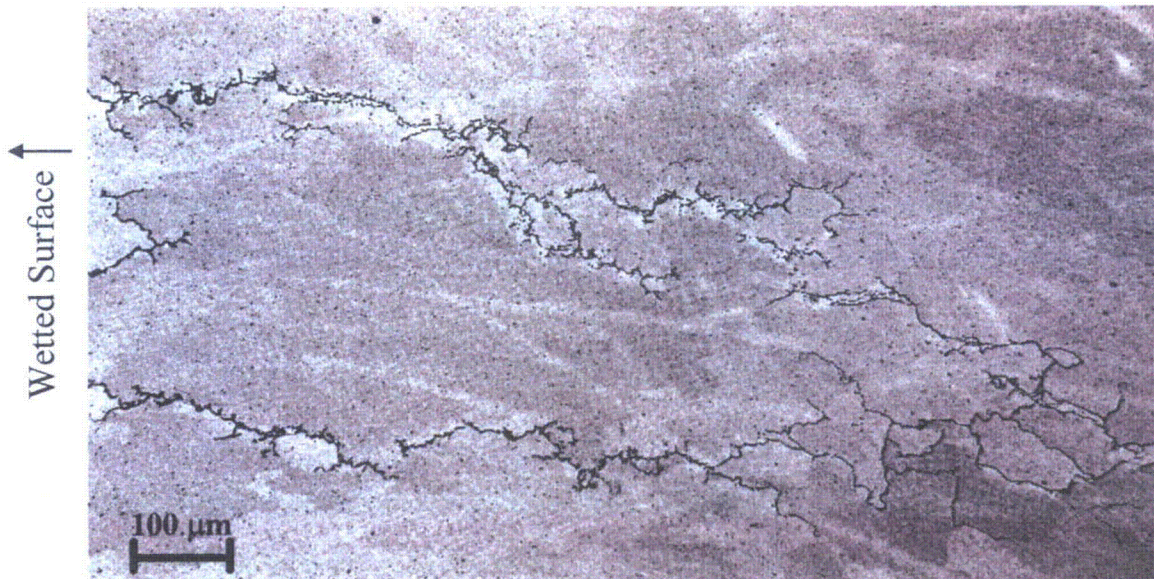


**Figure 6.29 Highly Branched Cracks Near Mid-Thickness in Cross-Section Sample A3**

After optical and SEM images were recorded on as-polished samples, several samples were given a two-step nital/orthophosphoric etch to highlight weld-metal microstructures. Typical examples are shown in Figure 6.30 for sample A5. The full crack montage in Figure 6.30(a) illustrates that the crack propagates through several different passes of the J-groove weld within the thickness of piece A. In most cases, crack openings appeared to be wider as cracks approached weld pass boundaries (Figure 6.30(b)). This may reflect the higher stress required to transition to a new set of interdendritic or grain boundaries. Significantly different orientations of the dendritic microstructure can be seen between weld passes. The crack path clearly followed interdendritic or grain boundaries, as documented in Figure 6.30(c). Tight secondary cracks meander along, and end on, the convoluted weld metal boundaries.

### **6.5.2.2 Metallography of Piece C Cross Sections**

The approach for metallographic characterization of the A cross sections was repeated for the C and E cross sections. Cracking was found to extend from the low-alloy steel interface all the way into the Alloy 600 tubing in the C samples, as indicated by the earlier optical examinations (e.g., Figure 6.17) before sectioning. This observation is confirmed in Figures 6.31, 6.32, and 6.33, where crack montages are shown for cross-section slices C1–C4, C5–C7, and C8–C10, respectively. The cracks in sections C1 and C2 end at the low-alloy steel interface with the Alloy 182 butter passes. Scanning electron microscopy micrographs of this region are presented in Figure 6.34, documenting that no propagation occurred into the low-alloy steel. A small pit can be seen, but no significant corrosion of the low-alloy steel.

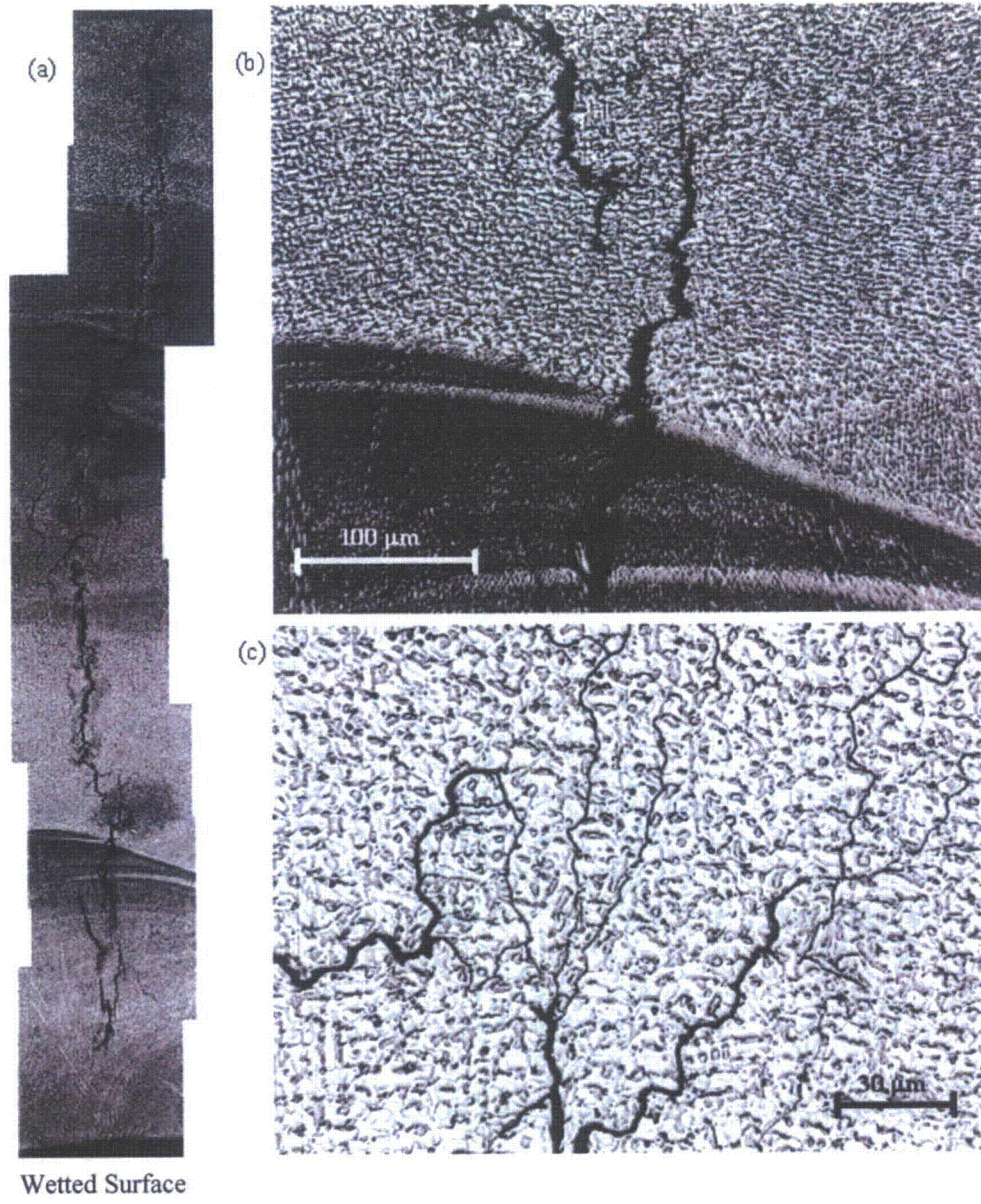


**Figure 6.30 Etched Microstructures in A5 Cross-Section Sample: (a) montage showing full length of crack; (b) example of more open crack near/at weld pass interfaces; and (c) example of cracks following convoluted boundaries**

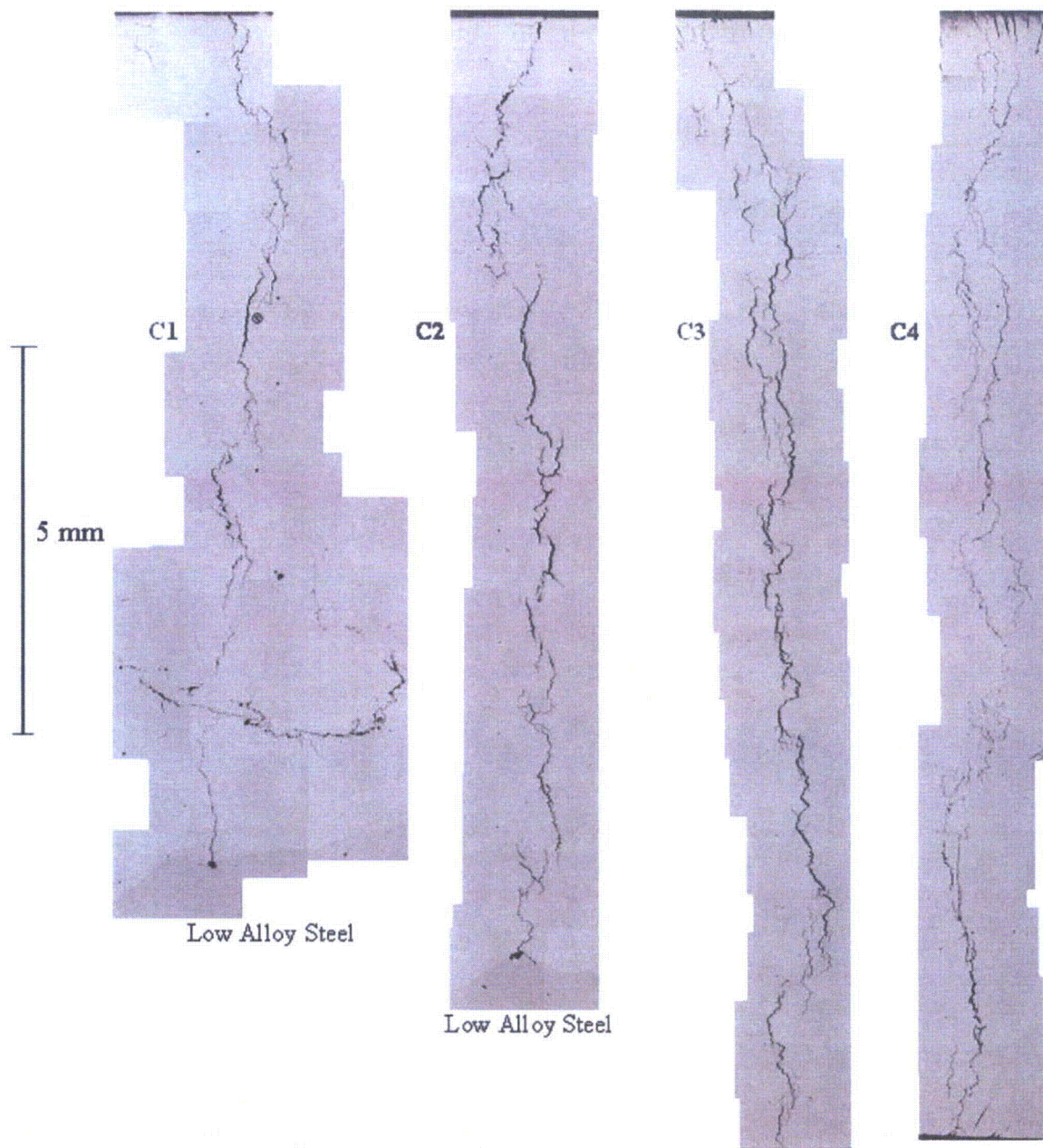


**Figure 6.31 C1, C2, C3, and C4 Cross-Section Samples Showing the Main Crack Running to the Low-Alloy Steel Boundary in C1 and C2, While C3 and C4 Show Crack Propagating Through Entire Thickness in Alloy 182 Weld Metal**

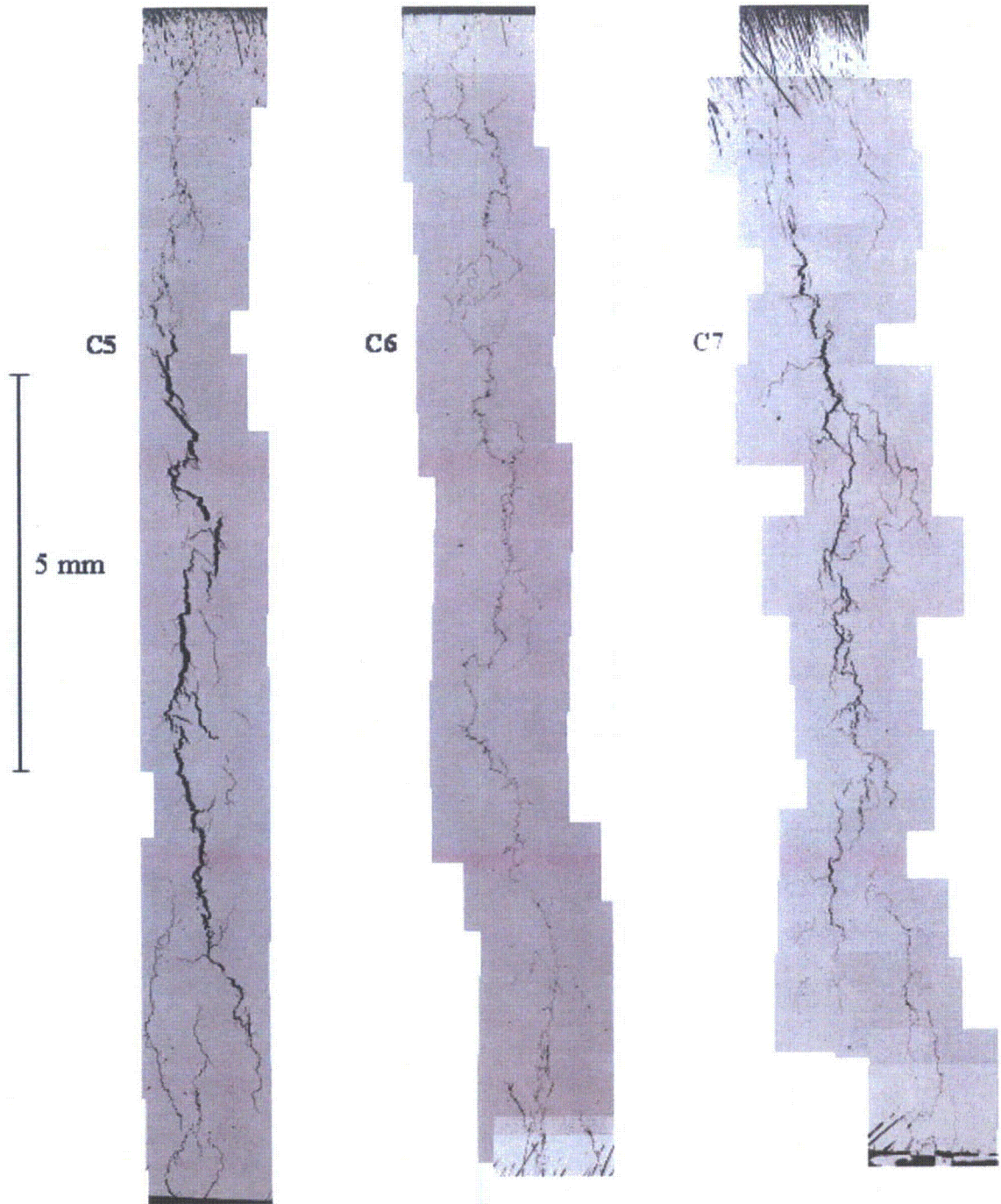


**Figure 6.32 C5, C6, and C7 Cross-Section Samples Showing the Main Crack Running Through Entire Thickness for These Locations**

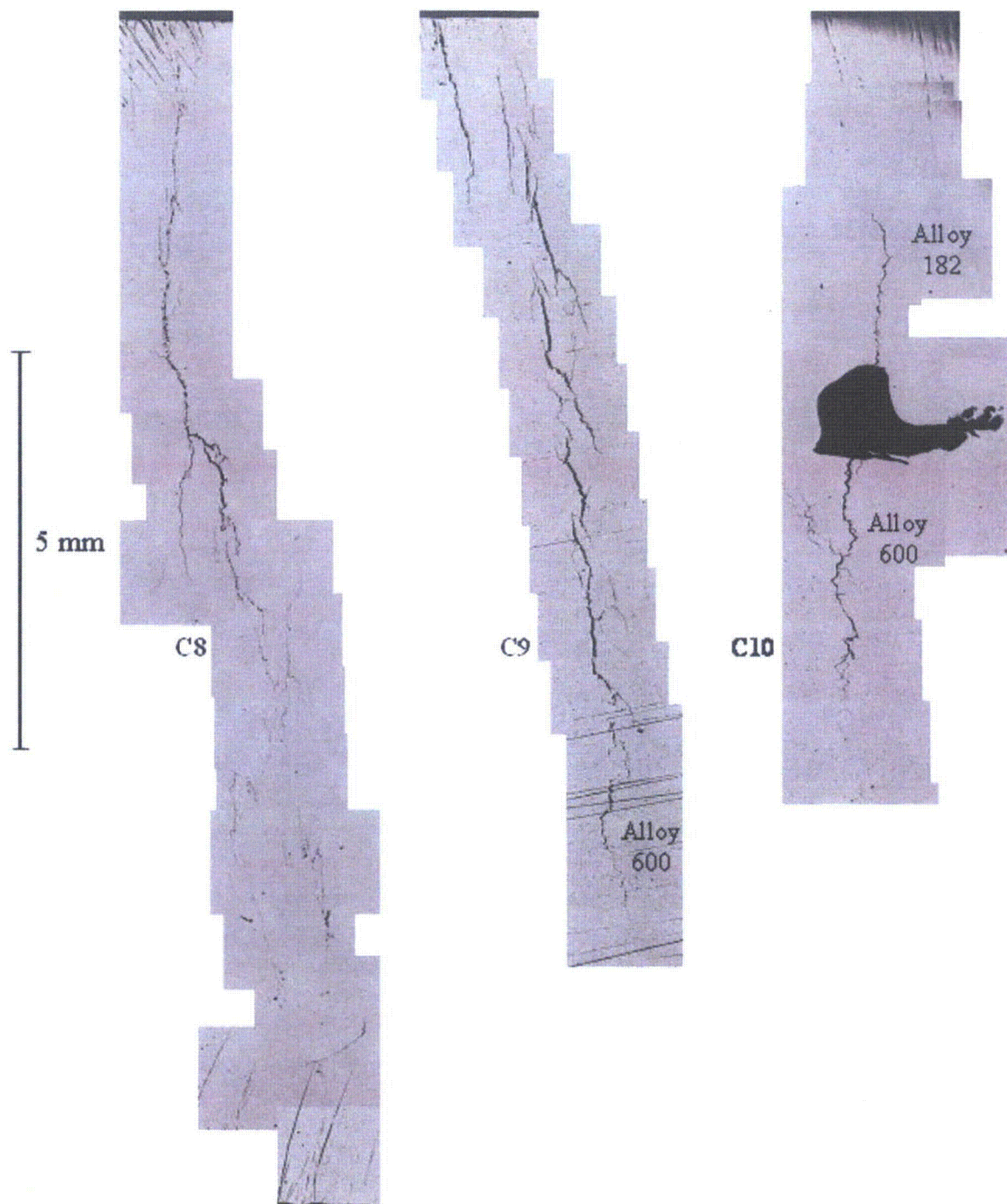


**Figure 6.33 C8, C9, and C10 Cross-Section Samples Showing the Main Crack Running Through the Alloy 182 J-Groove Weld into the Alloy 600 Tube. The large hole in the C10 cross section appears to be a weld defect at the alloy fusion line between the Alloy 600 tube and the Alloy 182 weld metal.**

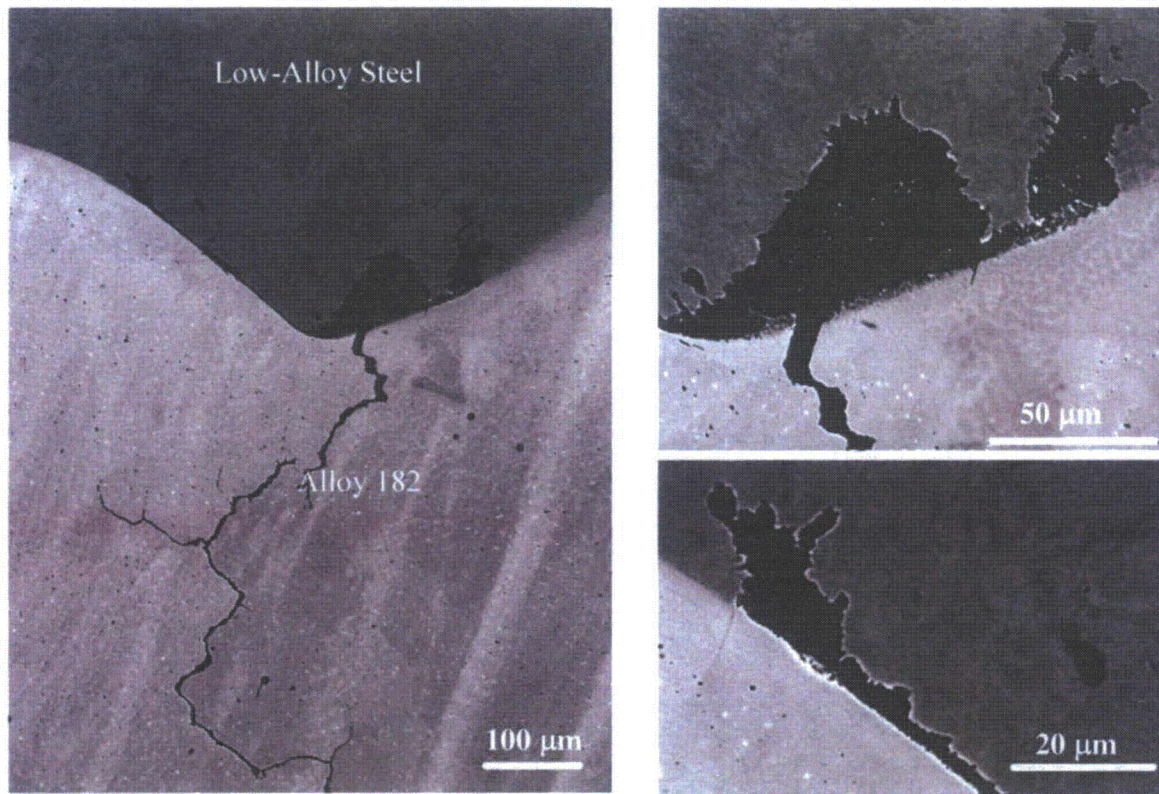


**Figure 6.34 Stress Corrosion Crack in Alloy 182 Butter Pass Ending at the Low-Alloy Steel Interface and Creating Small Corrosion Pits**

Similar to the microstructures documented for cross-section A5 (Figure 6.30), section C5 also was given an electrolytic etch using nital and orthophosphoric solutions. Although the exposure produced a heavy etch in places, the general microstructural features and the crack path could be recorded as illustrated in Figure 6.35. Once again, the SCC morphology is clearly interdendritic or intergranular following the convoluted boundaries in the Alloy 182 weld metal. Consistent with A5, wider crack openings were typically seen at the weld pass interfaces, with cracks often turning along the interface to find better-oriented boundaries for continued propagation. An example of this behavior is shown in Figures 6.35(b) and (c).

### 6.5.2.3 Metallography of Piece E Cross Sections

The final sequence of metallographic cross sections for piece E is given in Figure 6.36. This piece is split between the Alloy 182 butter passes and low-alloy steel plate. As a result, cracks are seen in only cross-sections E4 to E8 and propagate in only the Alloy 182 part of the way through the thickness before intersecting the low-alloy steel. Because the adjacent Alloy 600 tube was removed during initial cutting, E8 was the last slice that could be examined. The next sequential observation of the crack is from the exit surface into the interference-fit gap shown in Figure 6.23.

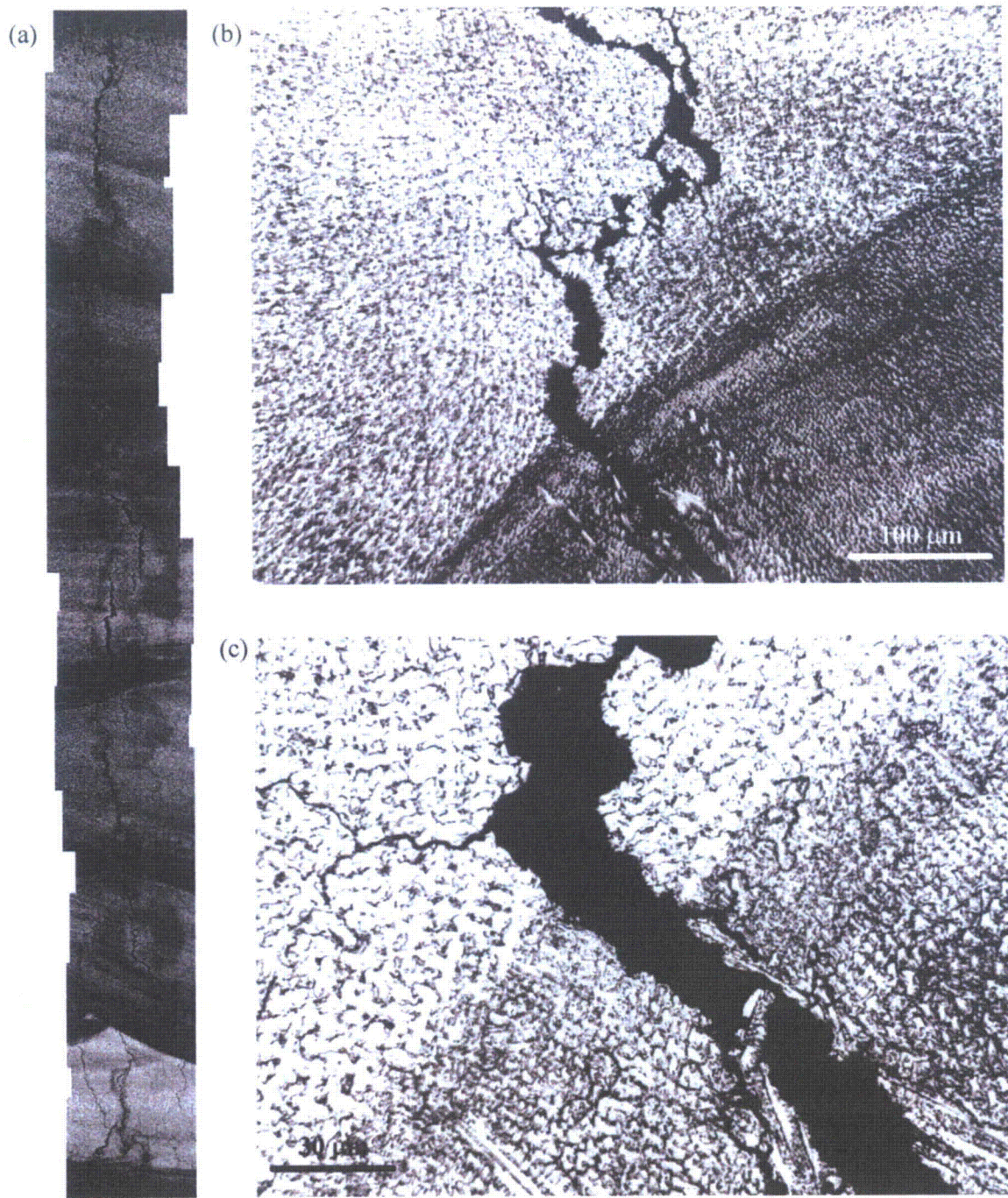


**Figure 6.35 Etched C5 Cross Section Showing Crack Propagating Through Many Alloy 182 Weld Passes**

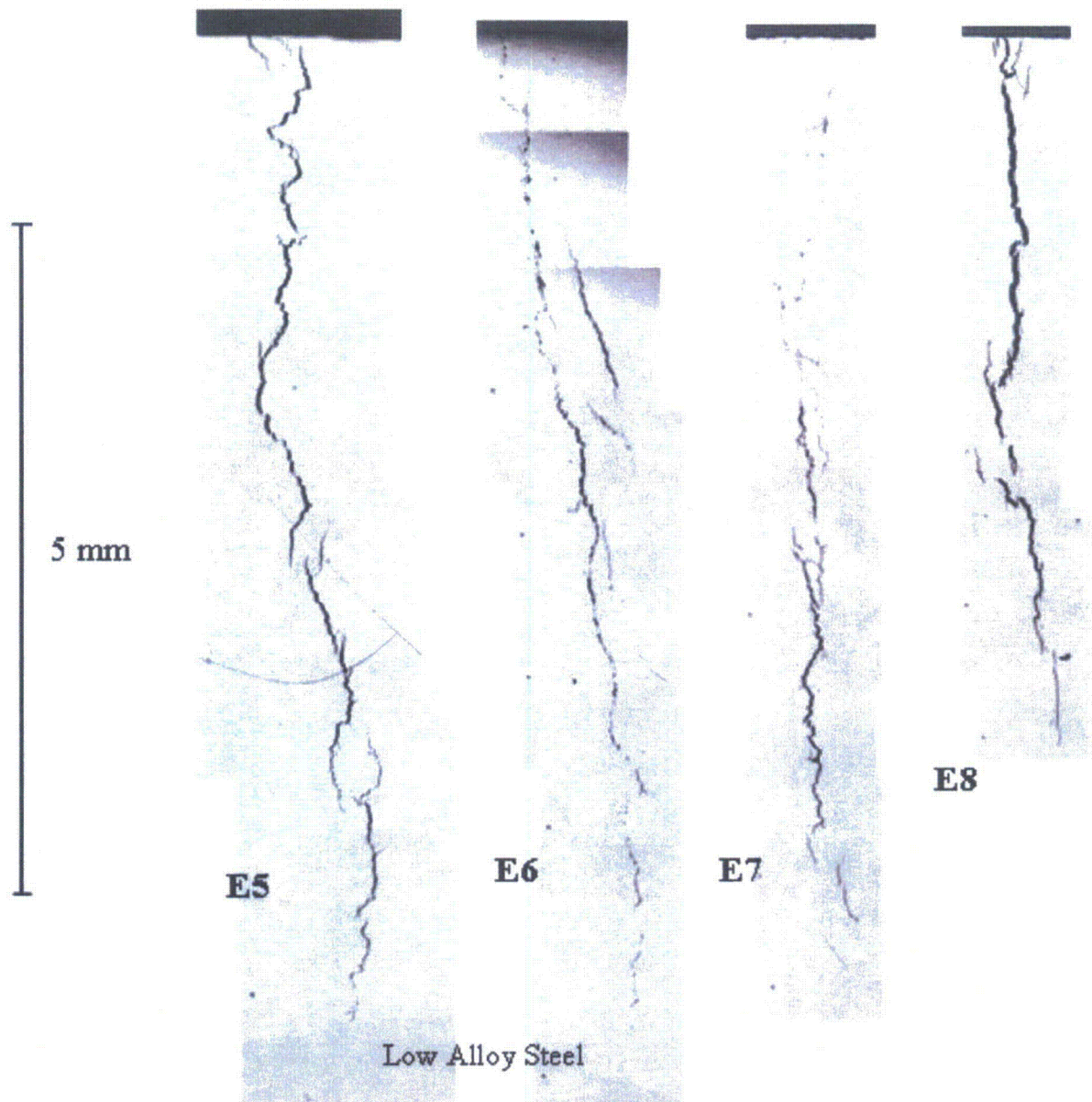


**Figure 6.36 E5, E6, E7, and E8 Cross-Section Samples Showing the Main Crack Running to the Low-Alloy Steel Boundary. Only a very small crack was seen in sample E4, and E8 was the closest slice to the gap surface.**

### **6.6 Metallographic Examination of Cracking in Nozzle 31 Section 3**

The detection of non-leaking cracks in Section 3 prompted its further cutting into smaller pieces for destructive examination. There are four cracks of interest in Section 3, at 200, 210, 225, and 255 degrees. The cracks at 200, 225, and 255 degrees have been confirmed as penetrating more than 6 mm (0.24 in.) into the weld. The crack at 255 was found to penetrate entirely through the weld and into the buttering past the triple point, but it does not intersect with the annulus.

The cracks at 225, 210, and 255 were imaged using SEM to determine their length and crack opening displacement. The crack at 225 is shown in Figure 6.37. The crack at 225 was found to have a length of 8.7 mm (0.34 in.) and a maximum COD of 30  $\mu\text{m}$  (0.0012 in.). The crack at 210 was found to be less than 6 mm (0.24 in.) deep via sectioning, but as it showed up in both PT and ET it was examined with SEM. The crack at 210 degrees has a COD of between 2  $\mu\text{m}$  (0.00008 in.). The crack at 210 degrees is shown in Figure 6.38.

The crack at 255 degrees was examined more extensively using SEM and sectioning. The first step was a careful examination of the wetted surface to locate the crack and trace it through the length of the weld. SEM of the wetted surface shows that the crack initiates at the boundary between the weld and the buttering, as with the leaking crack at 155 degrees. An optical image of the region near 255 degrees showing the crack profile on the wetted surface is shown in Figure 6.39.

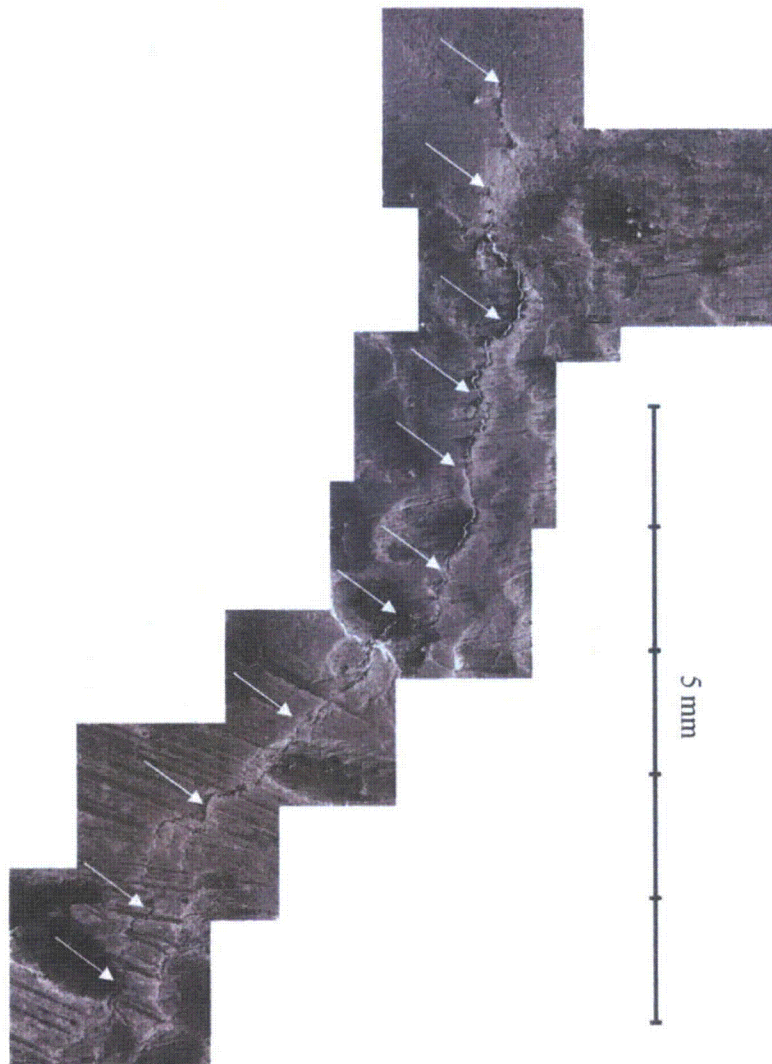


**Figure 6.37 SEM Image of Crack at 225 Degrees**

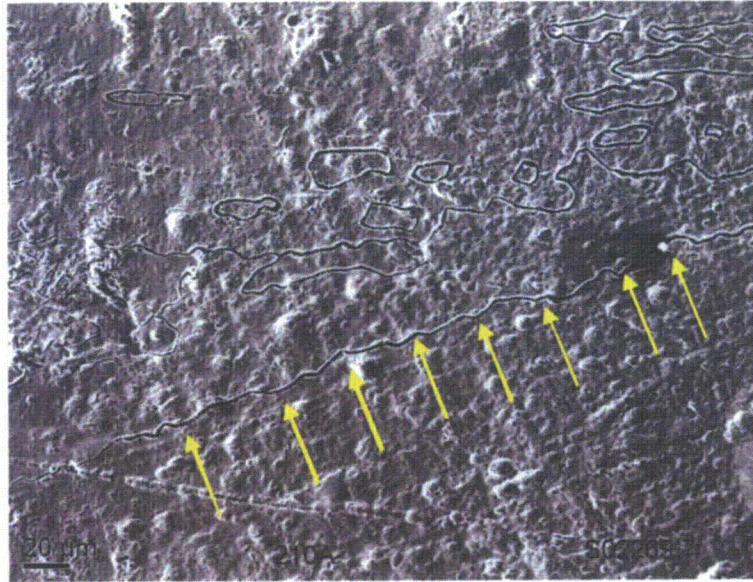


**Figure 6.38 SEM Image of Crack at 210 Degrees**

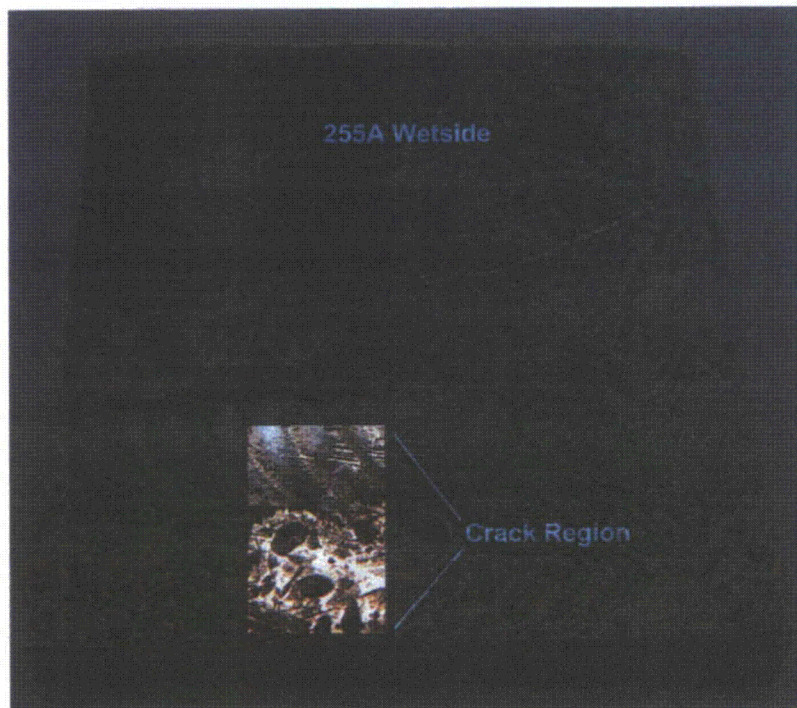


**Figure 6.39 Wetted Surface Location of Crack at 255 Degrees**

An SEM image of the 255-degree crack reveals a crack length of 7.6 mm (0.3 in.) and a COD of 40  $\mu\text{m}$  (0.0016 in.). The crack has a very broken profile, closing at several points along its length. The SEM image of the 255-degree crack is shown in Figure 6.40.

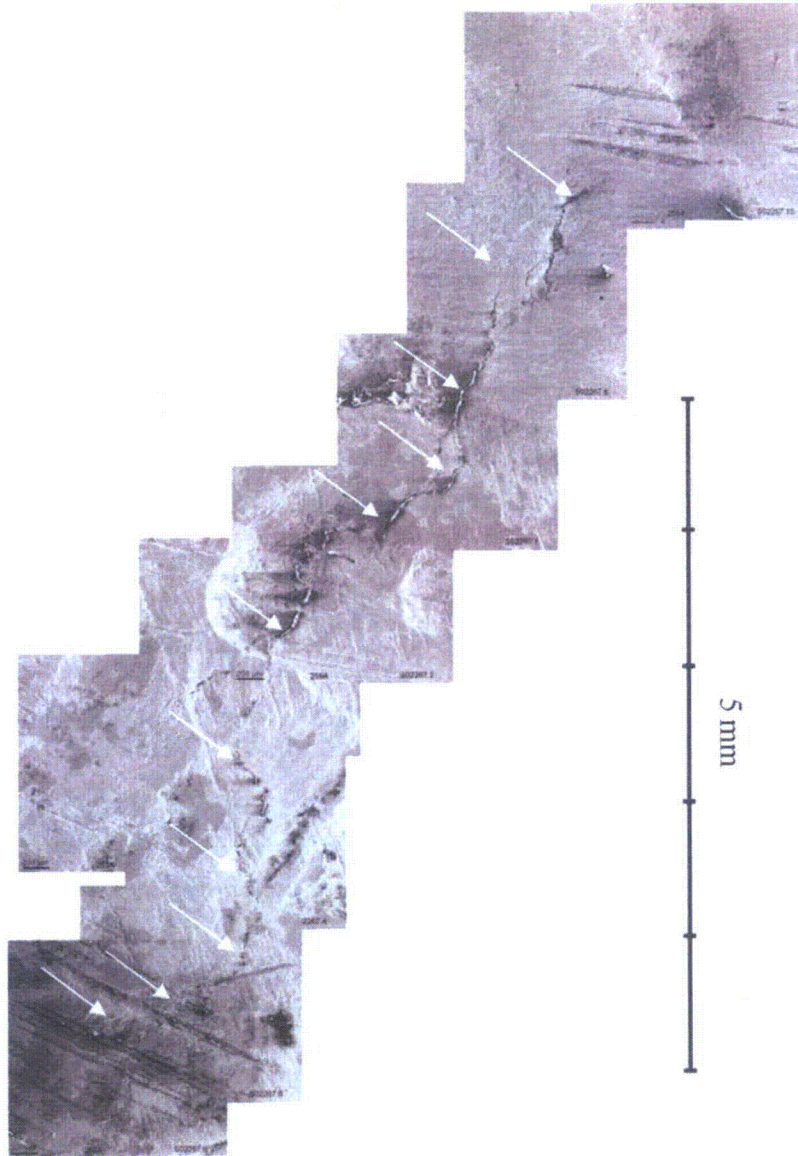


**Figure 6.40 Wetted Surface SEM Image of Crack at 255 Degrees**

The region around the crack was sectioned to allow a profile to be developed. The sectioning diagram and an image of the cut region are shown in Figure 6.41.

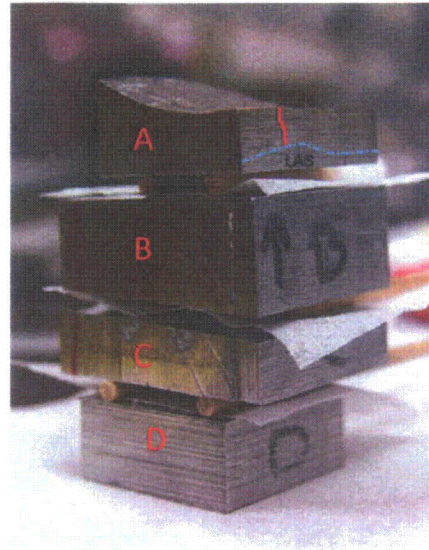
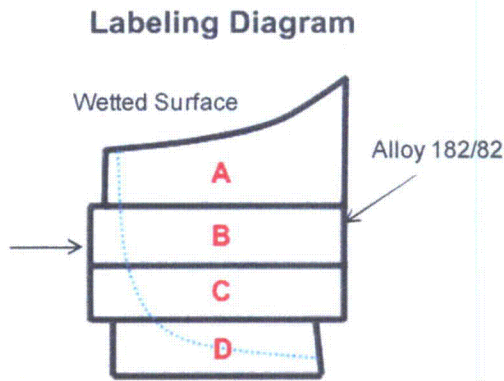


**Figure 6.41 Sectioning Diagram for the Region Around 255 Degrees**

The wetted-side faces of sections B, C, and D were polished and examined to determine the crack length and orientation at each face. The cracks at each face are shown in Figure 6.42.

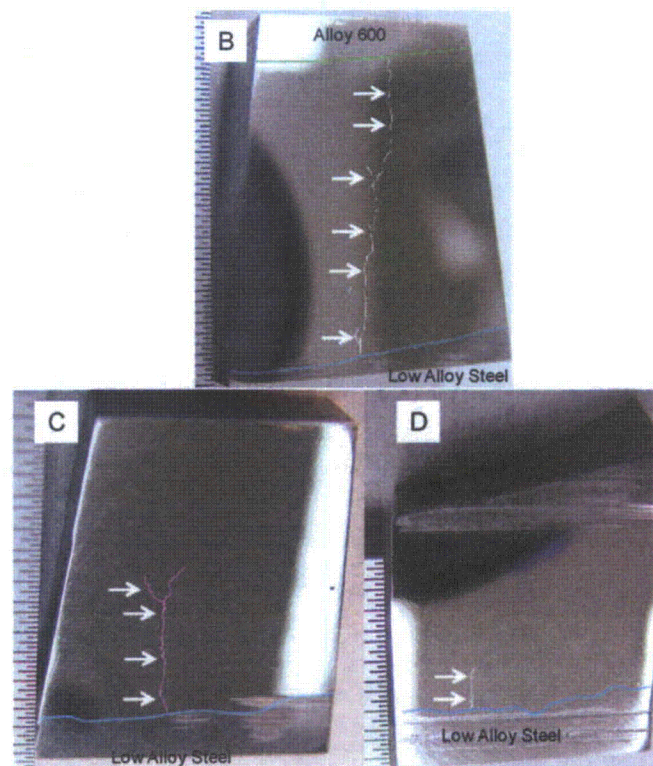


**Figure 6.42 Crack Locations at the Wetted Side Faces of Sections B, C and D of the 255-Degree Crack**

## 6.7 Destructive Evaluation Summary

The cutting of Nozzle 31 Section 2 revealed that the through-weld crack started at 155 degrees on the wetted surface at the weld-buttering interface and ended at 135 degrees above the triple point. Cutting this section also revealed two nearby cracks that had penetrated 8 mm into the material.

The metallographic characterization of the serial sections in pieces A, C, and E effectively mapped the cracks from their initiation in Alloy 182 weld metal on the PWR primary water surface to their end, either when intersecting with low-alloy steel, entering the Alloy 600 CRDM penetration tube, or exiting at the interference-fit gap above the J-groove weld. Cracking in Alloy 182 weld metal is interdendritic or intergranular and clearly has propagated due to stress corrosion cracking. No evidence for hot cracking in the weld was observed. Initiation appears to result from SCC near the fusion line between the butter passes and the J-groove weld. Surface damage and defects in the near-surface region may have promoted crack nucleation, but additional examinations will be needed to determine this.

The main crack is observed at a length of ~6 mm (0.23 in.) on the PWR primary water surface and expands to a lateral length of ~20 mm (0.78 in.) across the Alloy 182 weld metal within a few millimeters below the surface. At this depth, the crack already has reached the low-alloy steel plate material on one side and remains in the Alloy 182 J-groove weld on the other. Continued SCC propagation of the main crack extended its lateral length to ~25 mm (1 in.) at a depth of ~10 mm (0.39 in.), and it eventually reached the Alloy 600 CRDM penetration tube at a depth of ~17 mm (0.67 in.) in piece C. Limited SCC crack growth (few millimeters) into the Alloy 600 material from the alloy 182 is observed on two C cross-section samples. The extension of the main crack below the PWR primary-water surface finally ends in piece E when it again intersects the low-alloy steel plate at a depth of >30 mm (1.2 in.) and exits along the interference-fit gap on the side face. The main crack path length from the PWR primary-water surface initiation site to the gap-exit surface is estimated at ~25 mm (1 in.). Based on laboratory tests in simulated PWR primary water, typical crack-growth rates can range from  $\sim 3 \times 10^{-8}$  to  $\sim 3 \times 10^{-7}$  mm/s for as-welded Alloy 182 at 290 to 320°C. This results in an estimated time of ~2.5 to 25 years for the crack to propagate through-wall after initiation. Because crack initiation normally accounts for some important fraction of life, and through-wall cracking occurred at some time before its full 20-year life, the SCC crack-growth rate experienced in service was probably closer to the high end for measured propagation rates in the laboratory.

The interdendritic and intergranular SCC is highly branched, with tight secondary cracks along connected boundaries typically within a few hundred micrometers of the main crack. Many of these cracks appear to follow orientations nearly perpendicular to the main crack path, suggesting active propagation at somewhat low stresses. In addition to the main SCC crack through all three pieces, a second crack was observed in piece A at a distance of ~5 mm (0.20 in.) from the main crack. Surface examination and the cross-section samples indicated that this second crack also initiated at the PWR primary-water surface and propagated to a depth of ~10 mm (0.39 in.) within piece A. Macroscopic examinations suggested that this crack propagated into the adjacent piece B.

An overall image of the rendering that includes pieces A, C, and E is shown in Figure 6.43. One face of the weld section has been left out to allow viewing of the sections. As noted from the metallographic examinations, the crack rapidly expands from the initiation location on the PWR primary-water surface and spreads across the Alloy 182 weld metal reaching the low-alloy steel and Alloy 600. The green line indicates the boundary of the crack in the Alloy 182 weld metal, while the blue line indicates the crack

boundary where it arrested at the low-alloy steel interface. Red lines along the crack boundary indicate the points where the crack reaches the Alloy 600 interface and the interference gap (not shown) above the J-groove weld.

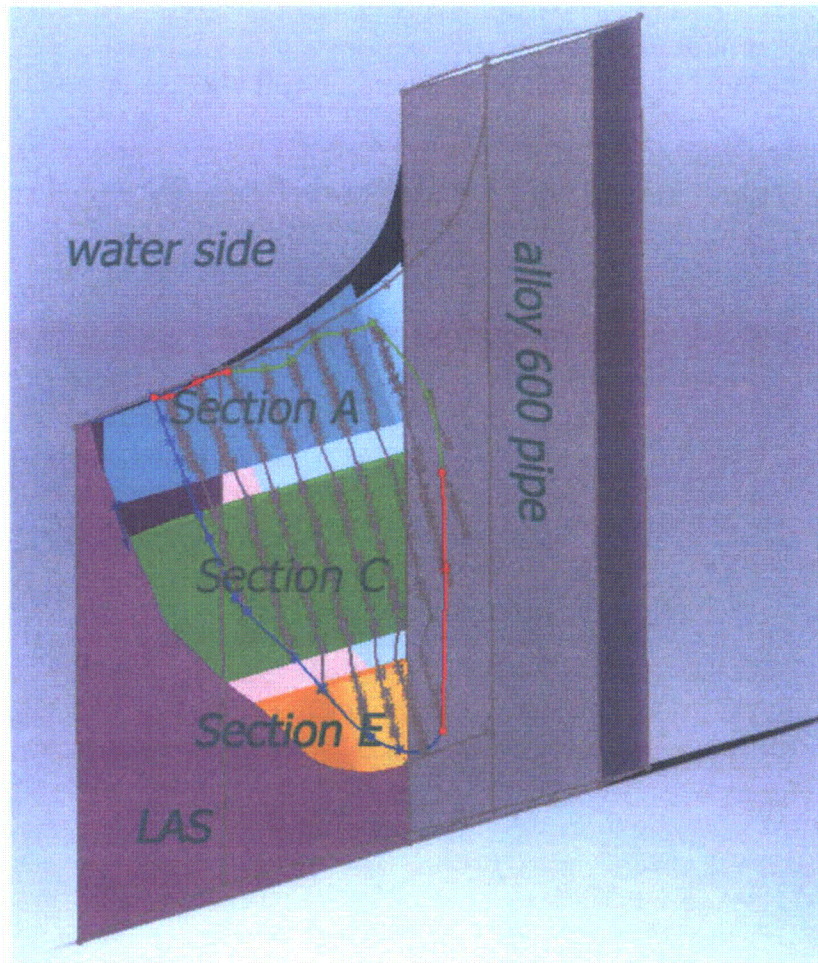


**Figure 6.43** Rendering of the Crack Within a Section of the Component Showing the Locations of Sections A, C, and E

Now that the basic framework has been created, much more detail can be built into this rendering to better elucidate the crack morphology through the weldment. Even at this stage, rotating the constructed image allows insights into the through-thickness crack path. For example, a nearly edge-on view of the crack is shown in Figure 6.44. Here it can be seen that the crack meanders during propagation through the weld material, possibly following the residual stress pattern. However, the path is relatively straight overall compared to component dimensions. In a more tilted orientation as shown in Figure 6.45, the small amount of propagation of the crack into the Alloy 600 pipe is more evident.

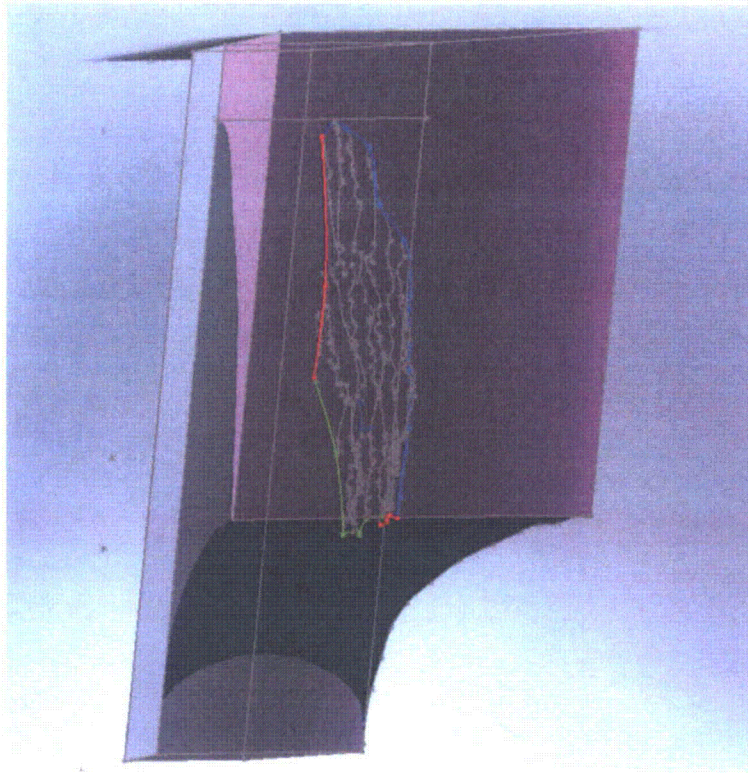


Figure 6.44 Crack Viewed from a Nearly Edge-On Orientation

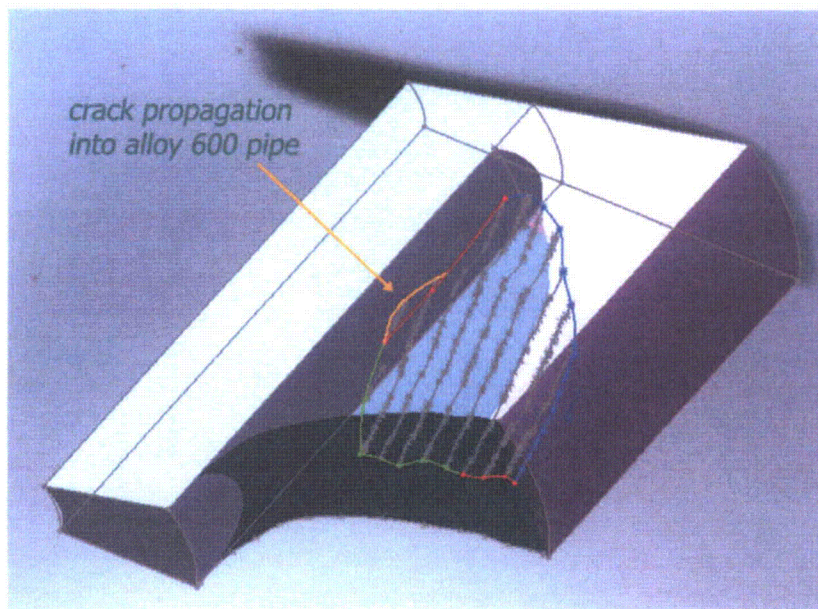
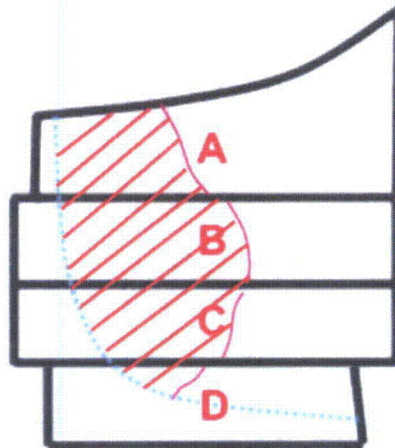


Figure 6.45 Component Section Viewed from a Tilted Orientation Where the Propagation of the Crack into the Alloy 600 Pipe Can Be Seen

A similar but less extensive reconstruction was performed for the deep crack located at 255 degrees. This crack is interesting in that it is one that may have leaked given more time but has not yet reached the annulus. The crack appears to propagate along the buttering/carbon steel interface and grow from this interface into the weld metal. As with the crack located at 155 degrees, the crack at 255 degrees is very short at the wetted surface and grows in length under the surface. A profile of the crack at 255 degrees is shown in Figure 6.46.

- A: Crack is 11mm long on cut side
- B: Crack is 15mm on A cut side and 18mm C cut side
- C: Crack is 17mm on B cut side and 10mm on D cut side
- D: Crack is 6 mm on cut side



**Figure 6.46 Reconstruction of the Crack as It Propagates Through the Weld Metal and Buttering**

## 7 Nozzle 54 Nondestructive and Destructive Examination Results

Nozzle 54 was examined nondestructively by the in-service examination teams, during the PNNL round-robin testing, and by Westinghouse. Westinghouse then examined Nozzle 54 destructively to characterize the cracking. The ISI and round-robin results are summarized in EPRI MRP 142 (EPRI 2005); the results for the Westinghouse examination of the nozzle and their analysis of the ISI, round-robin, and DE results are contained in EPRI MRP-198 (EPRI 2006). This section summarizes the ISI and round-robin results for Nozzle 54 and then compares these results to the Westinghouse NDE and DE results. For more detailed information on these results, non-proprietary versions of EPRI MRP 142 and 198 are available from EPRI.

### 7.1 In-Service and Round-Robin Nondestructive Testing Results

Nozzle 54 was inspected during the 2002 outage at North Anna Unit 2. The J-groove weld was inspected using ET. The penetration tube of Nozzle 54 was inspected ultrasonically and using ET. The annulus was ultrasonically inspected to determine if there were signs of leakage. The top of the nozzle was inspected for signs of boric acid deposits on top of the pressure vessel head.

The results of the in-service examination of Nozzle 54 were inconclusive. The bare metal examination of the nozzle showed no discernable leakage. The ISI examinations did find some ultrasonic indications at the interface between the nozzle OD with the J-groove weld and eddy current indications in several places at the outer portion of the crown of the J-groove weld. No leak path was found using the ultrasonic leak path examination technique. The ISI results are summarized in Table 7.1.

**Table 7.1 In-Service Inspection Results for Nozzle 54**

Description	Angle	Location
Ultrasonic indications	120–200°	Nozzle OD
	345–15°	Nozzle OD
Eddy current indications	115–140°	Outer half of weld wetted surface
	335–355°	Outer portion of weld wetted surface
	245°	Axial outer portion of weld
	200°	Axial nozzle ID location below weld

After the nozzles were cut from the pressure vessel head and shipped to PNNL, they were examined as part of a round-robin test held at PNNL by EPRI. The round-robin testing examined the penetration tube using ultrasound and eddy current techniques. The annulus of Nozzle 54 was examined using ultrasound and deep penetrating eddy current to search for signs of leakage or wastage in the interference fit that would be caused by primary coolant flowing through the interference fit if any leakage had occurred.

The round-robin testing of Nozzle 54 found many more indications in the penetration tube, and deep penetrating eddy current techniques found evidence of wastage in the annulus above the weld. Two eddy current indications were found in the penetration tube ID above the weld, which could lead to leakage if these indications penetrated through the tubing and into the annulus. A possible leakage path was also found using deep penetrating eddy current. The round-robin testing results are summarized in Table 7.2.

**Table 7.2 Round-Robin Testing Results for Nozzle 54**

<b>Description</b>	<b>Angle</b>	<b>Location</b>
Ultrasonic indications	350–20°	Penetration tube OD close to bottom of weld
	335–350°	Penetration tube OD bottom of weld
	130–200°	Penetration tube middle of weld
	120–220°	Penetration tube OD middle of weld
	60–180°	Penetration tube OD below weld
Eddy current leak path	350°	Penetration tube ID axial indication
	30–100°	Above weld in interference fit
Eddy current indications	155°	Tubing ID surface above weld
	220°	Tubing ID surface above weld
	240–250°	Tubing ID surface at bottom of weld

Based on these results, Nozzle 54 was chosen by industry for further NDE and destructive characterization.

## 7.2 Westinghouse Destructive Testing Results

After the round-robin testing was completed, Nozzle 54 was shipped from PNNL to Westinghouse for laboratory-quality nondestructive testing and destructive evaluation of the NDE results. A high-resolution replicant was applied to the J-groove weld surface of Nozzle 54 and the interior of the penetration tube of Nozzle 54. Nozzle 54 was then sectioned using a band saw into 12 pieces to allow for microscopic examination of the weld surfaces and an examination of the cut faces to determine the properties of the weld below the surface. Selected cut faces were milled to allow for highly sensitive ET, PT, and other examinations of the cut surfaces.

Cracking was confirmed in the outer portions of the J-groove weld crown of Nozzle 54. SEM examinations of the surfaces and the cut faces showed cracking at several locations around the outer regions of the J-groove weld in or near the buttering and penetrating into the buttering at some of the cut faces. The visual examination of the replica showed a string of defects from 270 to 60 degrees and individual defects at 70, 85, and 95 degrees. Some of the cracks were sectioned further and examined via microscopy and fractography. While some cracks were confirmed as PWSCC, none was more than a few millimeters deep, and all were contained in the buttering. No confirmation of deep cracking was found during the destructive evaluation of this CRDM.

The destructive evaluation agreed only partially with the ISI eddy current examination of the J-groove weld. Only one ISI ET indication was confirmed using SEM—the indication at 245 degrees. The string of ISI ET indications from 115–140 degrees is coincident with an indication at 135 degrees found using a replica of the weld surface. The J-groove weld results for Nozzle 54 are shown in Figure 7.1.

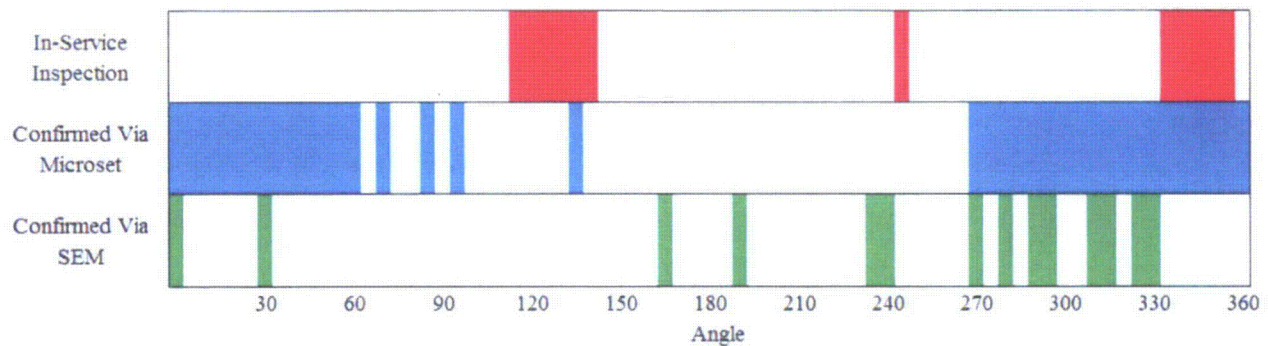


**Figure 7.1 Crack Indication Locations at Outer Region of J-Groove Weld**

Destructive examinations of the penetration tube found that the indications detected by ISI and round-robin testing were not associated with cracking but reflected fabrication conditions such as weld intrusion into the penetration tube and welding flaws. The eddy current indications found during round-robin eddy current testing were determined to be surface blemishes on the tube ID.

During the destructive evaluation, it was determined that there was no boric acid in the annulus and no signs of wastage of the carbon steel or of the penetration tube above the weld. The round-robin deep penetrating eddy current measurement showing wastage between 30–100 degrees was determined to be a false call. It is worth noting that the ultrasonic examination of the annulus did not detect any signs of leakage.

### 7.3 Nozzle 54 Summary

Because Nozzle 54 was not leaking and contained very little in-service degradation, the destructive analysis was useful in determining which fabrication conditions can cause false calls. The PWSCC present in the buttering region of Nozzle 54 had not penetrated deeply into the weld. The weld metal did contain several welding flaws, and the penetration tube surface was scratched and had other blemishes.

As with the ISI, round-robin, and PNNL examinations of Nozzles 59 and 31, the weld intrusions into the penetration tube of Nozzle 54 caused false calls during the volumetric examinations of the penetration tube. The eddy current examinations of the penetration tube ID found several indications that were caused by surface blemishes. These results are similar to the PNNL results for Nozzle 59, which was found to have scratches and rough patches but no cracks.

One interesting result of the SEM examinations of the wetted surface of the J-groove weld is that SEM found several cracks that were not detected by the ISI ET testing. Some of the flaws using SEM were very small, such as the flaw located at 235 degrees, which was less than 1-mm long and less than 10- $\mu$ m wide, but some others were over 3 mm long and over 100  $\mu$ m wide. EPRI MRP-198 (EPRI 2006) does not provide enough information to characterize each of the flaws found using SEM to determine which of those would be expected to be detected using field ET testing.



## 8 Discussion

The answer to the question of why some indications were detected through NDE and others missed becomes more clear when the nondestructive and destructive examination results are compared. The comparison also suggests ways to optimize future inspections of CRDMs and similar product forms. This section describes the NDE responses to the through-weld crack as well as the physical characteristics that caused these responses or lack of responses.

### 8.1 Important Characteristics of the Through-Weld Crack

Many aspects of the through-weld crack were discussed in Section 6. This section describes the crack characteristics specifically as they relate to the NDE techniques used to examine the CRDMs. There are three regions with different impacts to NDE detection—the appearance of the crack on the wetted surface, the crack characteristics for the first 3 mm, and the profile of the crack as it progresses through the weld. This section focuses on the through-weld crack in Nozzle 31 at 155 degrees.

#### 8.1.1 Crack Surface Characteristics

Scanning electronic microscopy of the wetted surface shows that the crack has a bent and discontinuous profile. Many separate and very tight cracks were found on the weld surface. A 4-mm-long (1.6-in.), 20- to 30- $\mu\text{m}$  (0.0008- to 0.0012-in.) COD discontinuous crack segment begins at the weld/butter boundary and extends at an angle into the buttering. A tail 2 mm (0.08 in.) long and very tight (too tight for the SEM to measure in many places) extends further into the buttering toward the stainless steel cladding. These features are shown in Figure 8.1. One important feature of the crack at the surface is its discontinuous nature. Even along the 4-mm-long main segment, there are several ligaments of metal crossing the crack. A section of the crack with several connecting ligaments is shown in Figure 8.2.

#### 8.1.2 The First Three Millimeters

As described in Section 6, the crack segments were polished and examined using SEM. The crack has a branching and discontinuous morphology in the through-weld orientation. Images of the crack and a color-coded image showing the various crack segments are shown in Figure 8.3. The first 3 mm show nine separate segments with ligaments between them. All the segments are part of the same crack, but they connect with each other outside the plane shown in the slice.

Also of interest is a detailed look at the crack COD at various points along the crack. Figure 8.4 shows the first 1.5 mm (0.06 in.) of the through-wall crack. Looking close to the surface, one finds several closed points very close to the surface of the crack. While the crack COD is 20–30  $\mu\text{m}$  (0.0008–0.0012 in.), the crack is much tighter—less than 0.10 mm into the weld.

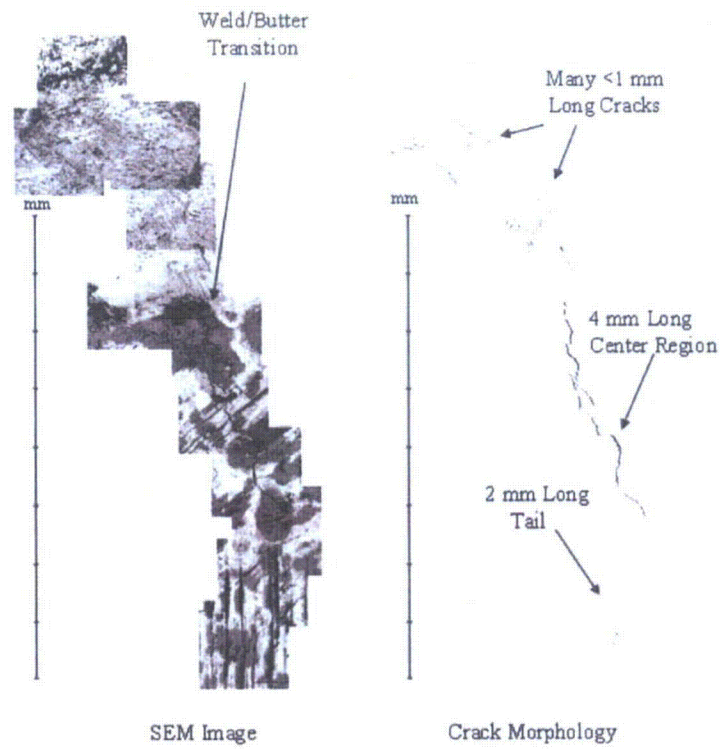


**Figure 8.1 Crack Image and Crack Morphology**

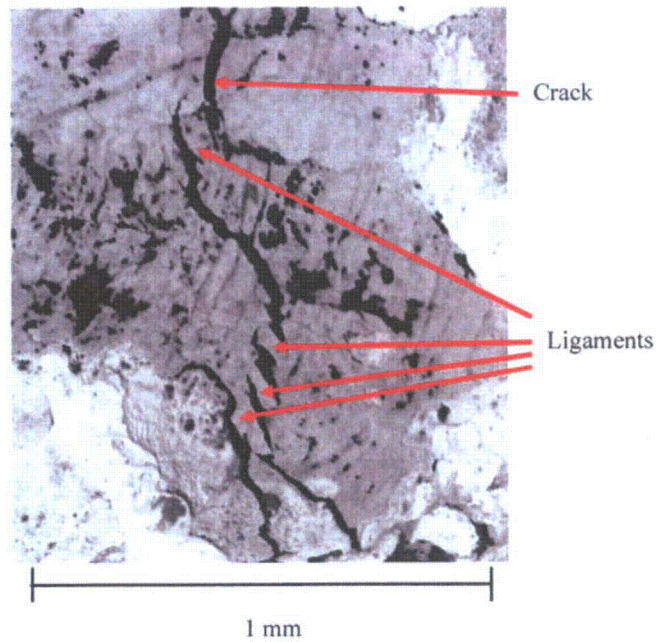


**Figure 8.2 Expanded Section of the Crack Showing Ligaments Bridging the Two Sides of the Crack**

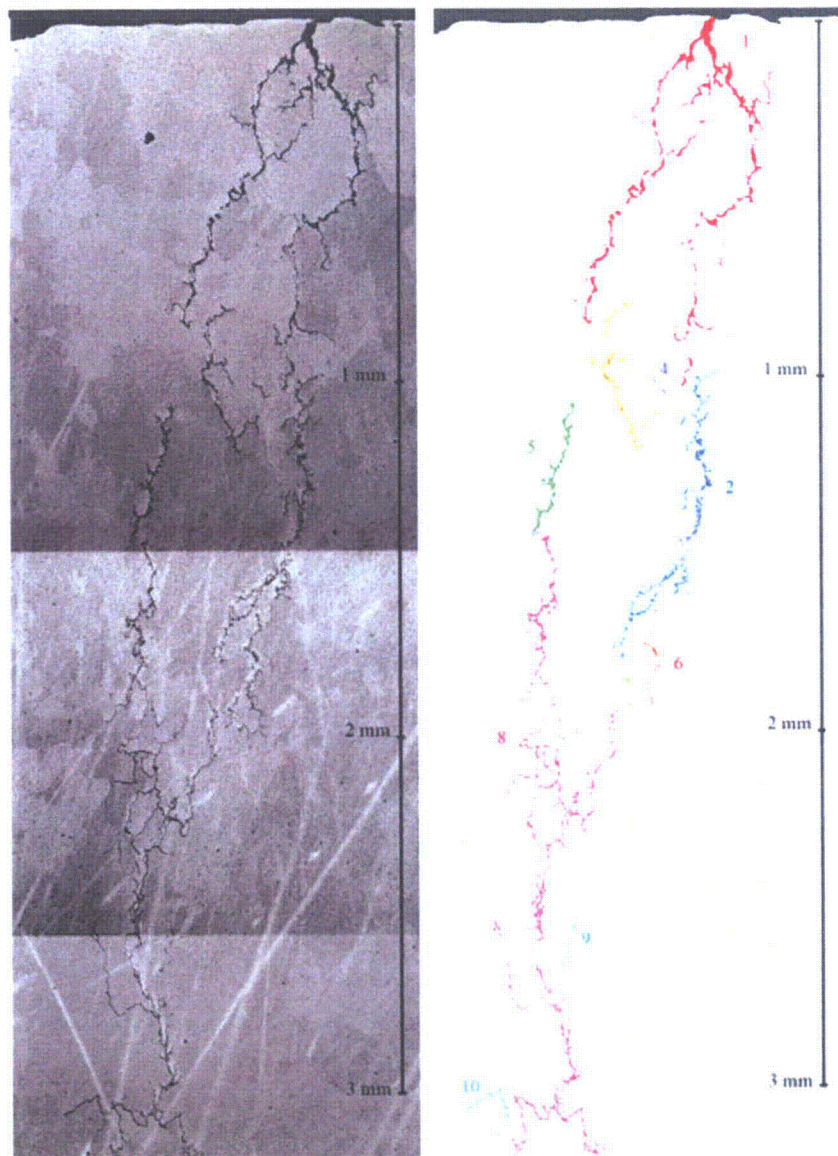


Figure 8.3 Crack Segments. SEM image (left) and color-coded image (right).

Location	COD ( $\mu\text{m}$ )
1	10
2	29
3	6
4	2
5	6
6	6
7	2
8	Closed
9	Closed
10	4
11	2
12	9
13	7
14	3
15	2



Figure 8.4 Crack CODs at Several Points Close to the Surface

### 8.1.3 Extent and Exit Point

The crack grew perpendicular to the wetted surface through the weld. The crack begins at 155 degrees on the wetted surface and exits into the annulus at 135 degrees. The crack is oriented axially almost directly, with only a 15-degree shift from a line perpendicular to the penetration tube at the cut 8 mm (0.30 in.) deep and directly perpendicular to the penetration tube at the triple point. Although the crack looks very branched and spread out in the SEM images, it is less than 1 mm across along its length. For any technique looking through the penetration tube, the crack presents a knife's edge to the tube. The exit into the annulus happens along almost the entire length of the buttering, from above the triple point to the carbon steel. The crack exit into the annulus is 15  $\mu\text{m}$  (0.0006 in.) at its widest point.

## 8.2 Effects of Crack Morphology on Nondestructive Examination Responses

A re-evaluation of the NDE responses in the context of the known location and morphology of the through-weld flaw is very illuminating. Knowing the location and morphology of a leaking crack essentially "unblinds" the NDE results and allows for a clear discussion of the strengths and weaknesses of each technique.

## 8.2.1 Time-of-Flight Diffraction

Time-of-flight diffraction examination was not performed on the J-groove weld, and this work obtained no DE-verified data on the use of TOFD to detect and characterize PWSCC. The TOFD technique could be useful to detect and size PWSCC in the J-groove weld if some development work were done to perform TOFD on this area. The largest barriers to using TOFD on the J-groove weld are the surface conditions, the difficulty of projecting ultrasound through the weld metal, and the geometry around the weld. Significant development work needs to be done before TOFD is usable on the J-groove weld, but it would provide a volumetric verification for ET.

## 8.2.2 Zero-Degree Ultrasonic Testing

The ultrasonic inspection of the J-groove weld yielded no discernable signal from the through-weld crack. The UT data for the region around 135–155 degrees does show some likely fabrication flaws similar to the fabrication flaws found in the DE, such as in slice C10 (Figure 6.33). This lack of signal from the crack is interesting, as the crack is directly against the penetration tube for most of its length. The UT calibrations and the imaging of fabrication flaws in Nozzles 31 and 59 show that the UT can image small defects at the same depth into the weld metal. Even knowing exactly where to look, using the most sensitive frequency at the correct depth (5 MHz) and using high gain, it is not possible to find any significant crack signal. Figure 8.5 shows the 5-MHz results in the cracked area of the J-groove weld. The crack is in an unfavorable orientation, essentially presenting a knife's edge to the beam, which likely accounts for the lack of signal. It was known that the UT inspections would be less sensitive to an axially oriented flaw, and this has been confirmed by these inspections. Performing a UT inspection through the J-groove weld would need to use different angles to be sensitive to the axial cracks present in the weld.

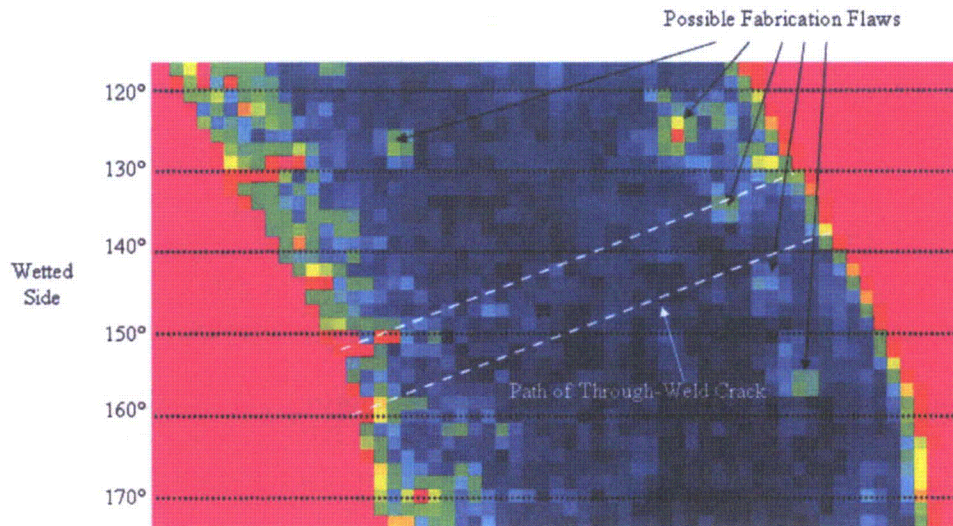


**Figure 8.5** 5-MHz Ultrasonic Testing Data for the Cracked Region of the Nozzle 31 J-Groove Weld Metal

The zero-degree ultrasound was effective at detecting fabrication flaws. Some of the UT indications were intersected by the saw cuts. The cut faces showed the presence of welding flaws. One such exposed welding flaw at 15 degrees is shown in Figure 8.6.

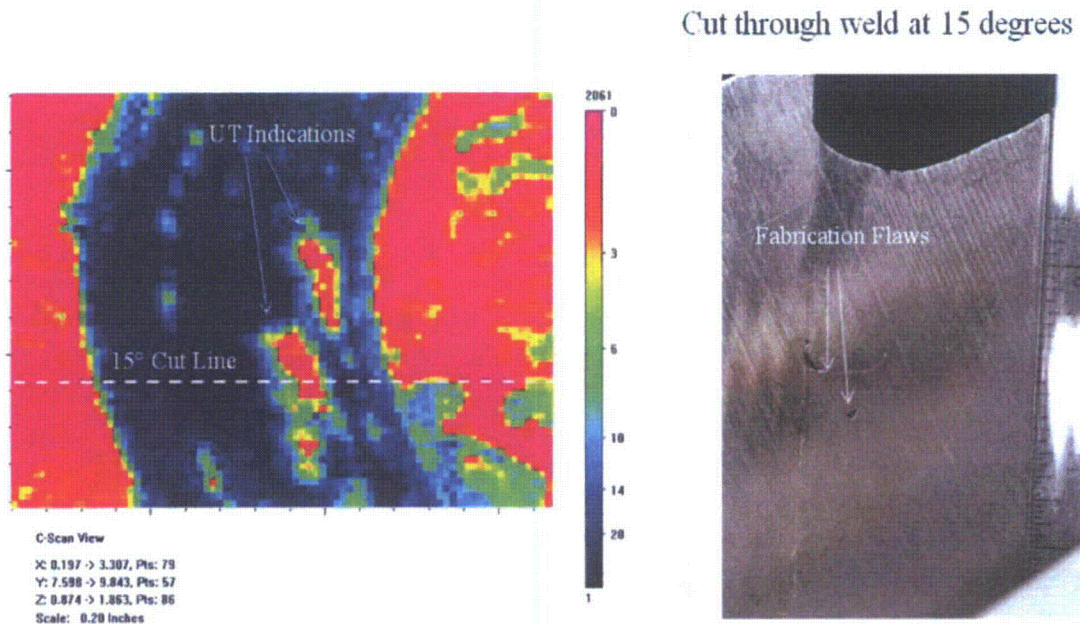


**Figure 8.6 PNNL UT Results Showing the Cut Line at 15 Degrees and the Cut J-Groove Weld Surface**

It is worth noting that the PNNL, round-robin, and ISI ultrasonic examinations missed the presence of the cracks at 145, 155, 160, 200, 225, and 255 degrees. The crack at 155 degrees was completely through the weld and leaking, and the crack at 255 degrees was through the weld and into the buttering. However, these results are not unexpected because the orientation and location of the flaws made them very challenging for UT to detect them reliably.

### 8.2.3 Visual Testing via Replication

The results from the visual testing using a replicate as a primary crack detection technique were somewhat disappointing. The replicant material did a very good job of capturing surface features, and the replica imprint also likely includes the cracks. The largest problem encountered was the limited ability to discern scratches and innocuous features from cracks. Finding the very tight cracks is complicated by the presence of many larger features. This work used a high-resolution digital camera to investigate the replica, and it is possible that the use of SEM would improve the ability to discriminate between cracks and other features. Using the camera and careful examination of the images found none of the actual cracks, and all indications found using this technique were confirmed as scratches or weld irregularities by ET, PT, and bare-metal VT.

The replicate testing was very useful in following up the ET examinations of the penetration tube in Nozzle 59. The replicate allowed us an alternative examination technique to determine what had caused the ET responses in the tube.

One factor that made the replicate testing difficult was that the J-groove weld surface was in the as-welded condition. The lines between the weld passes and the borders of weld beads made many distracting linear indications that may confuse the inspector and camouflage cracks.

#### **8.2.4 Penetrant Testing**

The PT performed on the J-groove weld of Nozzle 31 yielded interesting and complex results. The PT results showed conclusively that some cracks were present in the weld, where they were, and that many of the indications found using VT to test the replicate were not cracks. The PT results helped to guide the bare-metal VT testing. Also, the PT result for the crack at 210 degrees was used to set the lower voltage response level used to interpret the ET testing results.

The PT testing did not, however, yield any signal at the site of the through-weld crack. Three reasonably deep (>8-mm [0.31-in.]) cracks were centered around 150 degrees, yet none of them was detected using PT. This suggests that even very deep PWSCC can be missed by high-sensitivity PT testing. A higher-quality inspection surface may help improve the reliability of the penetrant inspection.

#### **8.2.5 Visual Testing via Macro Photography**

The visual testing was not very reliable because the cracks were very tight and the surface of the J-groove weld was mottled and uneven. The region near 0 degrees was difficult to inspect at an optimal angle until the penetration tube was removed, which is not a viable option for ISI. The bare metal visual was able to confirm the cracks at 200 and 225 degrees, but it was not able to find the through-weld crack at 155 degrees. The cracking near 155 degrees was difficult to image, even in an optical microscope, and images usable for COD determination were really obtainable only using a scanning electron microscope. These results suggest that visual testing in the field would be very difficult and that the detection of tight cracks on an as-welded surface is unlikely to be reliable.

High-magnification optical images of the surface near the crack show that the black oxide and surface features make it difficult to detect the crack with visual techniques. One would expect that a 25- $\mu\text{m}$ -wide crack would be easily visible on a good surface, but the color changes and difficult surface morphology (small dents and apparent grinding marks) effectively mask the crack to direct visual inspection. These surface features also make it difficult to find the crack using replicant techniques such as the Microset replicant. An image of the surface containing the crack is shown in Figure 8.7.

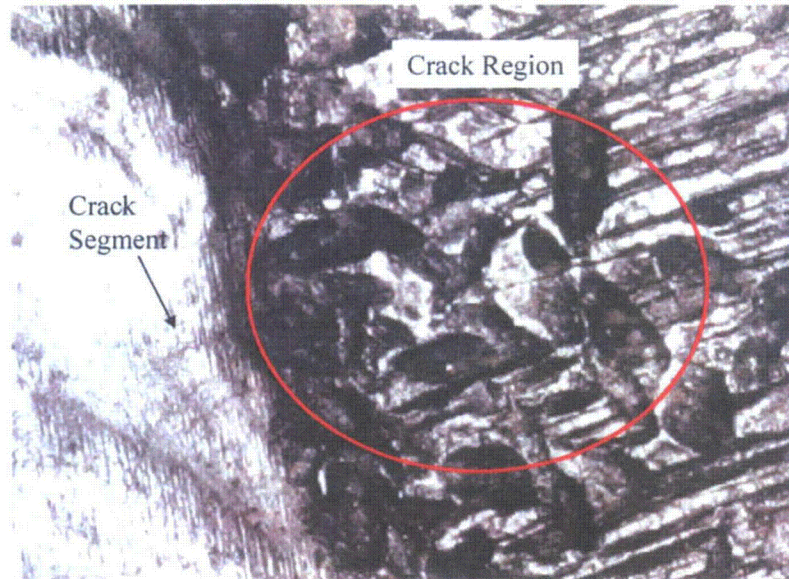


**Figure 8.7 Cracked Region with Poor Crack Detection Because of Surface Features and Oxides**

It is possible that the reliability of bare metal visual testing would be improved by having a higher-quality inspection surface. The unground as-welded condition was difficult to inspect and provided a large number of distracting indications that can help camouflage a crack.

### **8.2.6 Eddy Current Testing**

ET was the one technique that was able to detect the through-weld crack in the J-groove weld of Nozzle 31, as well as all of the cracks detected using PT and VT. The ET scan of the J-groove weld helped to pinpoint several crack-like indications for further investigation. The ET on the J-groove weld of Nozzle 31 was the most sensitive examination used and yielded the most reliable results. The ET testing results were verified using PT and VT and by cutting the nozzle under the indications to visually expose the cracks. The compiled ET indications are described in Table 8.1. The indications are described by the angle at which they were found, the length of the indication, the amplitude of the indication relative to an EDM notch, if the flaw was detected by in-service inspection, and the approximate depth of the crack if it is confirmed to be a crack.

The verified ET results show that the ET indications exhibit amplitudes greater than 30% of the reference EDM notch and a length greater than 7 mm. The unconfirmed indication at 55 degrees had an amplitude of 32% but a length of less than 4 mm.

One interesting result is that the ET response to the through-weld crack (3.1 V) was lower than the responses for some of the shallower cracks (4.1–4.6 V). The discontinuous, segmented nature of the through-weld crack, both on the surface and along the crack depth, allows for electrical contact between the two crack faces. This electrical contact is the most likely reason for this lower ET response. This segmented nature reduced the signal by approximately 1–1.5 V or reduced the ET response by 25% to 38% of the calibration response for the reference notch.

**Table 8.1 Compiled Flaw Information for ET Indications in Nozzle 31**

Indication	Angle	Length	% EDM Notch	Called by ISI?	Verified Depth
1	45°	2 mm (0.078 in.)	20%	No	Less than 6 mm
2	50°	5 mm (0.20 in.)	18%	No	Less than 6 mm
3	55°	4 mm (0.16 in.)	32%	No	Less than 6 mm
4	65°	2 mm (0.078 in.)	18%	No	Less than 6 mm
5	70°	4 mm (0.16 in.)	21%	No	Less than 6 mm
6	75°	3 mm (0.12 in.)	24%	No	Less than 6 mm
7	80°	3 mm (0.12 in.)	22%	No	Less than 6 mm
8	130°	4 mm (0.16 in.)	22%	No	Less than 8 mm
9	145°	10 mm (0.39 in.)	31%	No*	Between 8 mm and 25 mm
10	155°	8 mm (0.31 in.)	32%	Yes	Through-weld leaking
11	160°	14 mm (0.55 in.)	40%	No*	Between 8 mm and 25 mm
12	170°	5 mm (0.20 in.)	25%	No*	Less than 8 mm
13	200°	8 mm (0.31 in.)	45%	Yes	Between 6 mm and 25 mm
14	215°	10 mm (0.39 in.)	18%	No	Less than 6 mm
15	225°	9 mm (0.35 in.)	45%	Yes	Between 6 mm and 25 mm
16	255°	7 mm (0.28 in.)	41%	Yes	Through-weld not leaking

\* Flaw not called but a review of the ISI data shows an ET indication at this location.

In Nozzle 54, the effectiveness of ET is not as clear. Many cracks found using SEM were not called by ET testing, and areas called as flawed by ET did not show significant cracking using SEM and visual testing via replicant. Many of the flaws found by SEM may have been too small for ET to reasonably detect, but not enough information was present in the EPRI MRP-198 (EPRI 2006) to determine the crack lengths.

The largest drawback of the ET scans was that differential ET used to examine the weld is not able to measure the depth of an indication to detect much of the subsurface extent of the flaw. The differential probes are sensitive to only the first 3 mm and missed the much longer parts of the cracks that were below the surface. The ET scans using the differential probe provided the locations of the crack but were not able to identify which of the flaws was the leakage path. The determination of which flaw was the through-weld flaw relied on cutting above the triple point with the saw, which is not a feasible ISI technique.

### 8.2.7 Leakage Path Measurements

Both PNNL and ISI ultrasonic scans were able to detect physical features in the annulus caused by the leakage of borated water through the interference fit. During the destructive examination of Nozzle 31, the penetration tube was removed from the annulus and the ID of the annulus was photographed. The carbon steel was cut into sections to allow the removal of the penetration tube. The first observation was that the annulus contained boric acid deposits. Two areas appeared to be possible leakage paths. At 45 degrees, one finds a channel worn into the steel of the annulus. This water path also shows on the penetration tube. A section of the penetration tube was recovered and photographed and is shown in Figure 8.8.

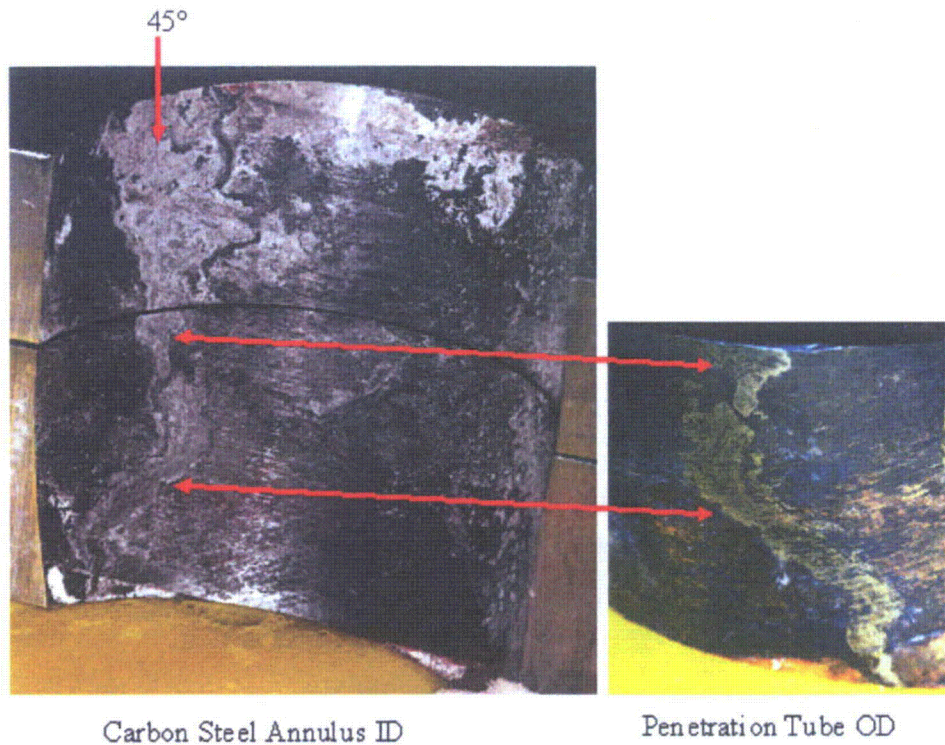


**Figure 8.8 Mirror-Image Damage to the Carbon Steel Annulus and a Section of the Alloy 600 Penetration Tube. The wetted surface is toward the top of the samples.**

A large and complex boric acid deposit was found ranging from 90 to 270 degrees. This boric acid deposit is shown in Figure 8.9 and Figure 8.10. Again the wetted side is at the top. The entire length of the annulus is present from approximately 100–180 degrees, with the small section containing the leak removed for destructive evaluation. Coolant had clearly leaked through this region, leaving the boric acid deposits. A “clean” channel with no boric acid starts at 90 degrees and bends around to 135 degrees at the “exit” point out of the annulus. It is not known if this “clean” band is a region where extra water flowed through the interference fit or a region where no water flowed.

Evidence for coolant flowing through the boric acid deposits is observed in the “clean” regions of the carbon steel annulus. Apparent wastage of the carbon steel is evident at close to 180 degrees. This is shown in Figure 8.11. There is also visible evidence for coolant flowing through the clean region, as shown in Figure 8.12.

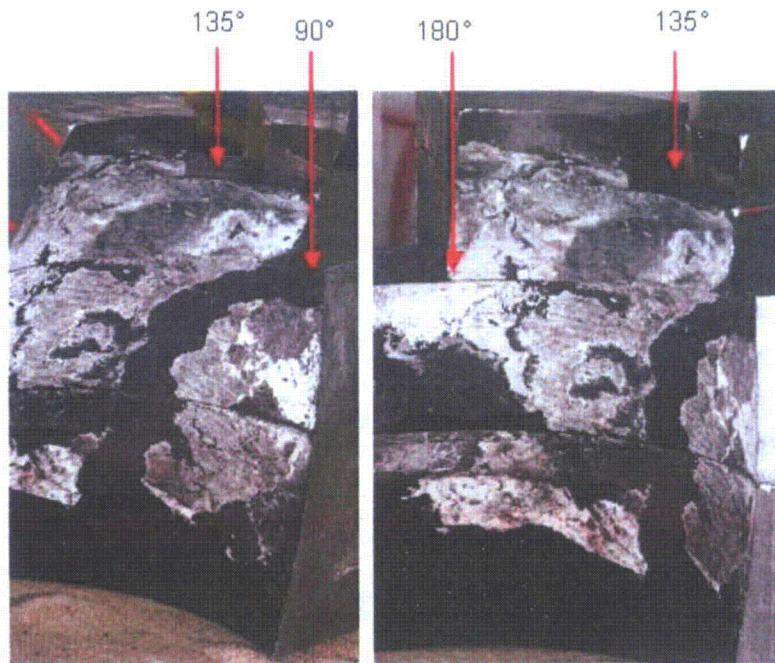


**Figure 8.9** Boric Acid Deposits on the Carbon Steel from 90–180 Degrees. The wetted surface is toward the top of the samples.

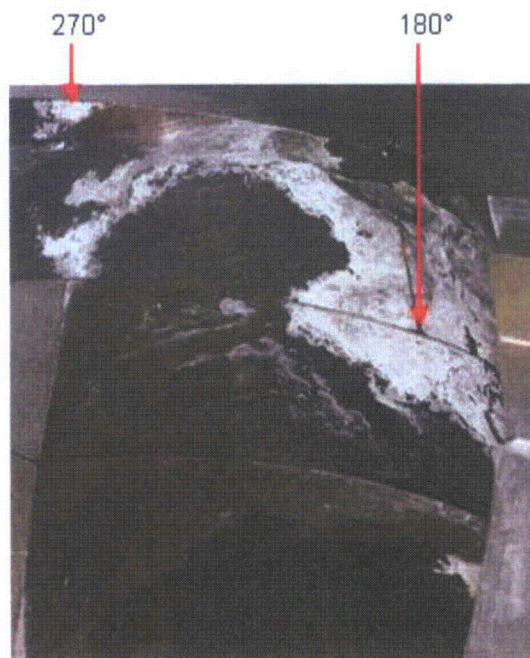


**Figure 8.10** Boric Acid Deposits on the Carbon Steel from 180–270 Degrees. The wetted surface is toward the top of the samples.

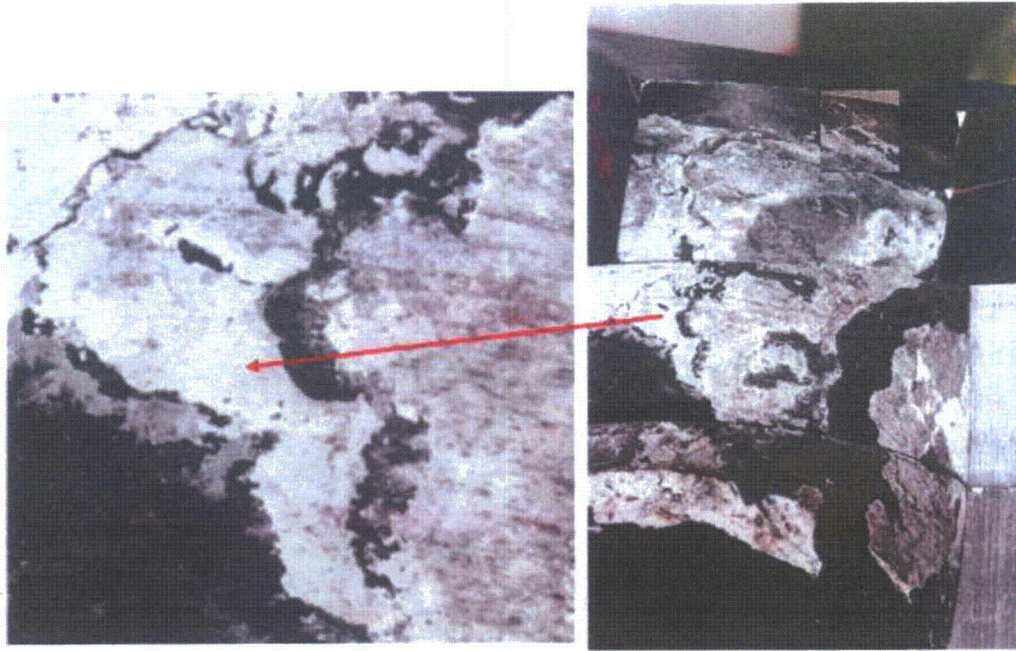


**Figure 8.11 Enlarged Region Showing Damage to the Metal in the Boric Acid-Filled Region**

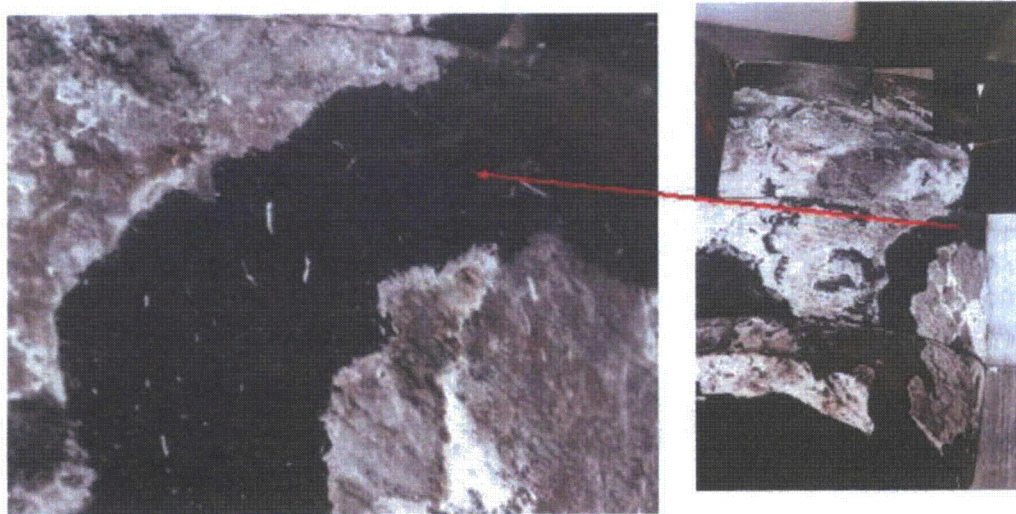


**Figure 8.12 Apparent Water Flow Damage in the "Clean" Region of the Annulus**

The ultrasonic data of the annulus and interference fit were obtained by PNNL while examining the J-groove weld. The data obtained by PNNL and industry (Figure 5.21) were very similar and showed the same pattern, including the river delta and apparent exit path. The industry-acquired data on the interference fit are shown in Figure 5.21. The data acquired by PNNL, with the region of interest focused on the annulus region, are shown in Figure 8.13. The ultrasonic data taken at PNNL were optimized for the J-groove weld, and the signal in the interference fit is often saturated, making it less quantitative.

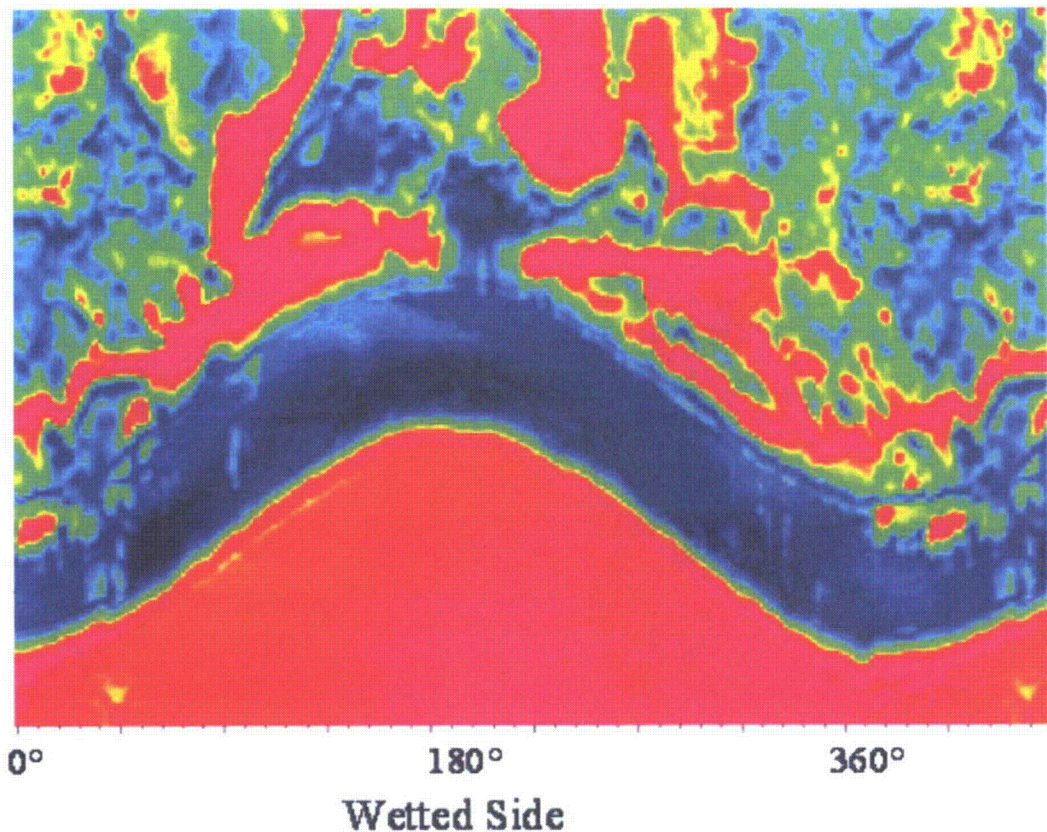


**Figure 8.13 PNNL-Acquired Data on the J-Groove Weld and Part of the Interference Fit of Nozzle 31 After the Nozzle Had Been Removed from the Head**

Despite the different techniques and goals, there are many similarities between the PNNL and industry data. Both data sets find the same pattern and the same signal that was called as a leakage path. When the ultrasonic data and the photographs of the annulus are compared, it is clear that the pattern of the boric acid deposits matches the ultrasonic data patterns. The called leakage path corresponds directly with the clean band in the annulus that starts near 90 degrees. Some of the other features in the boric acid deposit patterns are replicated in the UT data as well. Some correlations between the UT data and the boric acid pattern are shown in Figure 8.14.

Although the boric acid patterns show up very well in the UT data, the leakage path at 45 degrees is not visible. The UT data and the carbon steel annulus near 45 degrees are shown in Figure 8.15.

It is also useful to compare the results of a confirmed leaking nozzle such as Nozzle 31 with a likely non-leaking nozzle. PNNL performed similar UT examinations on Nozzle 59, which did not appear to have any through-weld leaks. The UT pattern in the annulus was very different than in Nozzle 31. In Nozzle 31, the UT revealed a complex pattern where the UT signal is transmitted and reflected, while in Nozzle 59, the annulus appeared to be a good reflector of ultrasound almost everywhere in the annulus. The difference in UT patterns is shown in Figure 8.16.

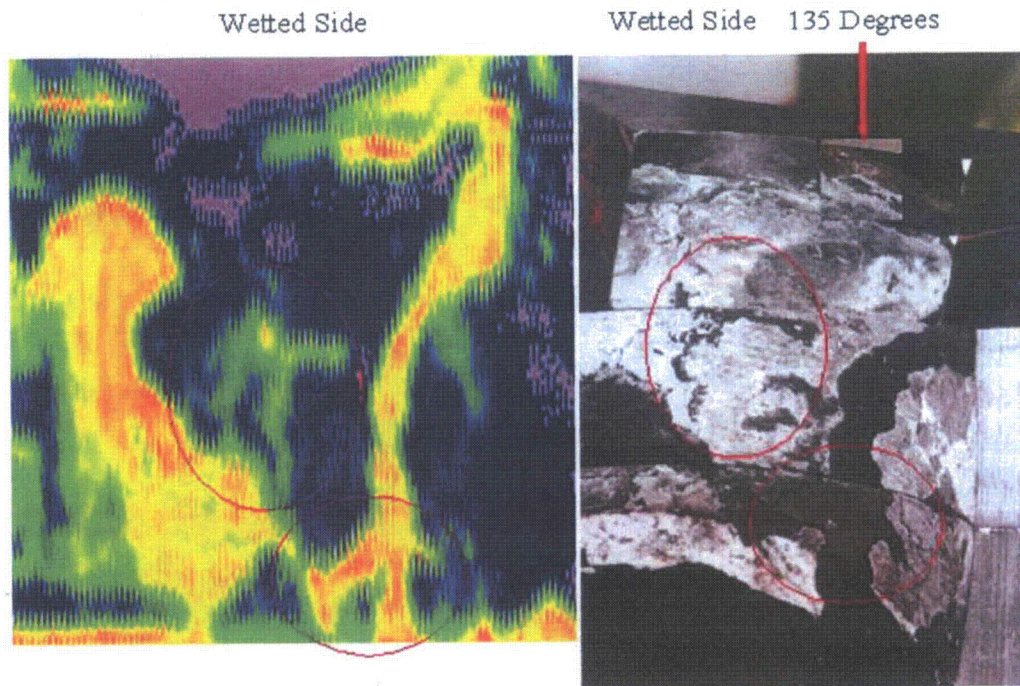


**Figure 8.14** Comparison of Boric Acid Patterns on the Carbon Steel Annulus and UT Patterns on the Left

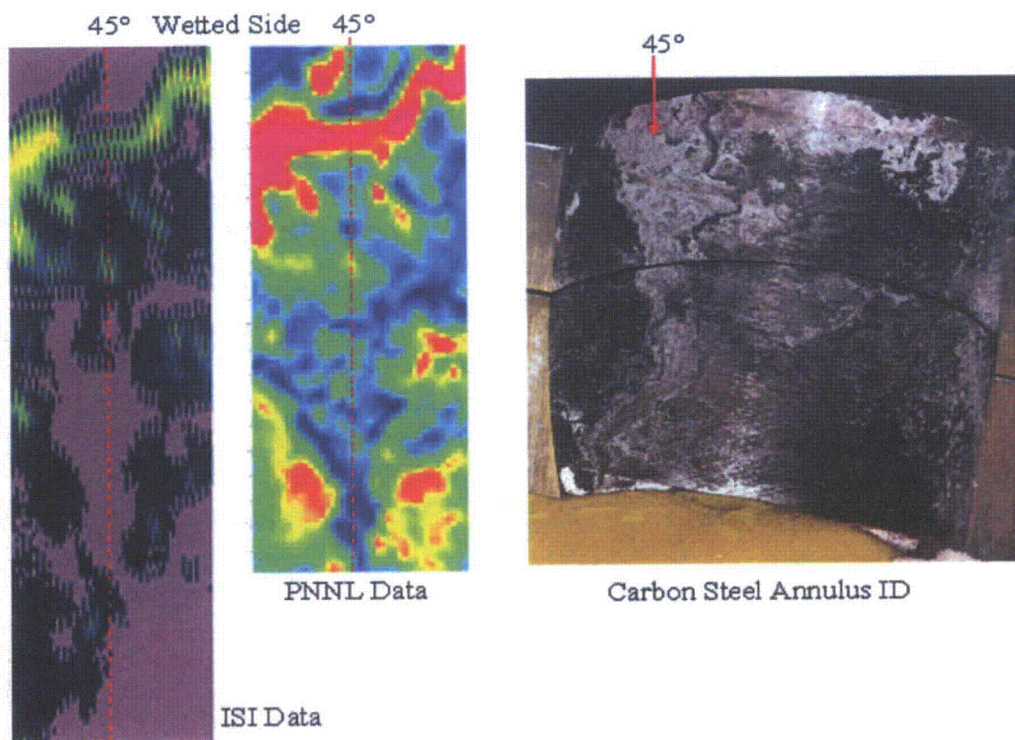


**Figure 8.15** Comparison of the UT Data and the Apparent Wastage of the Carbon Steel Near 45 Degrees

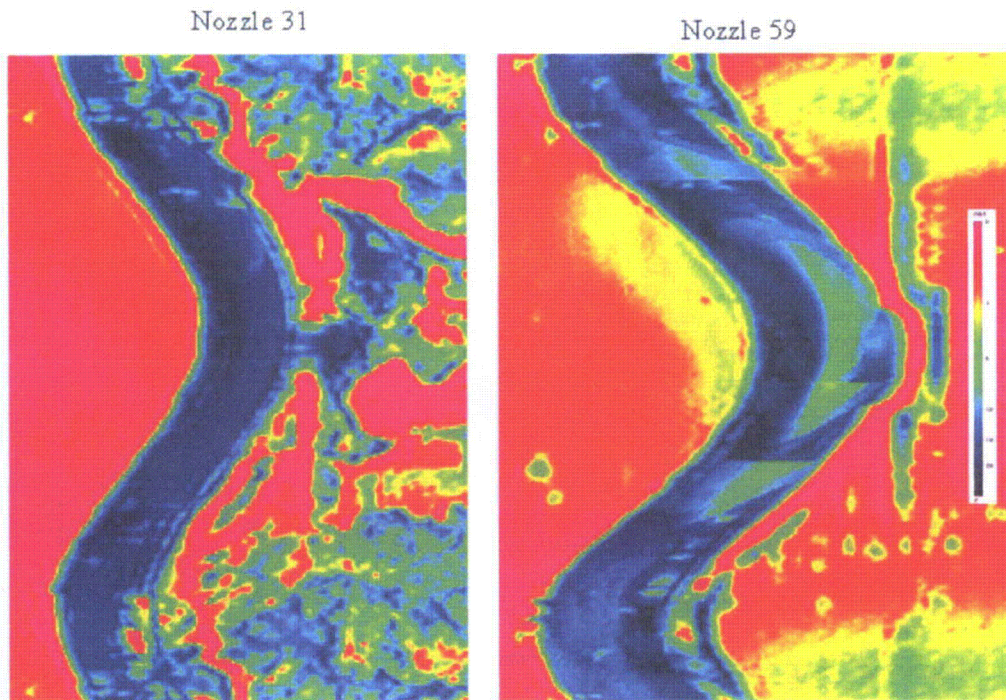


Figure 8.16 Comparison of the UT Patterns Found for the Interference Fit in Nozzles 31 and 59

### 8.3 Integrated Results and Suggestions

Inspecting Alloy 600 and 182 weld metal for PWSCC is difficult because of the complex geometry at the weld, the materials, the tightness of the cracks, and the short length the cracks present at the initiating surface. All six cracks confirmed by DE and deeper than 6–8 mm (0.25–0.30 in.) were all axially oriented, making the volumetric inspections performed through the penetration tube ineffective. The cracks are so tight where they break the surface that VT and PT are of very limited usefulness because both techniques missed the through-weld flaw.

The only technique that was able to detect the through-weld flaw in the J-groove weld was ET. It would be very helpful to have an additional technique capable of examining the J-groove weld and buttering. If developed, a radially oriented TOFD capable of characterizing axially oriented flaws would possibly be able to verify and depth-size PWSCC in the weld region.

The characterization of the through-weld flaw showed an interesting and important aspect of PWSCC—that the flaws can be very short on the surface and span the width of the weld within a few millimeters. A very deep crack can appear as a very small indication to surface techniques such as VT or PT and near-surface techniques such as ET. Penetrant dye testing indications that may be ignored as weld porosity and short, low-voltage ET indications need to be considered important.

As short, low-voltage ET indications are possibly important, work could be done to use ET to characterize fabrication flaws and noise levels in CRDM welds to prevent false calls based on innocuous indications. A detailed understanding of ET noise levels and common fabrication flaws would be very useful in examining data collected in the field.

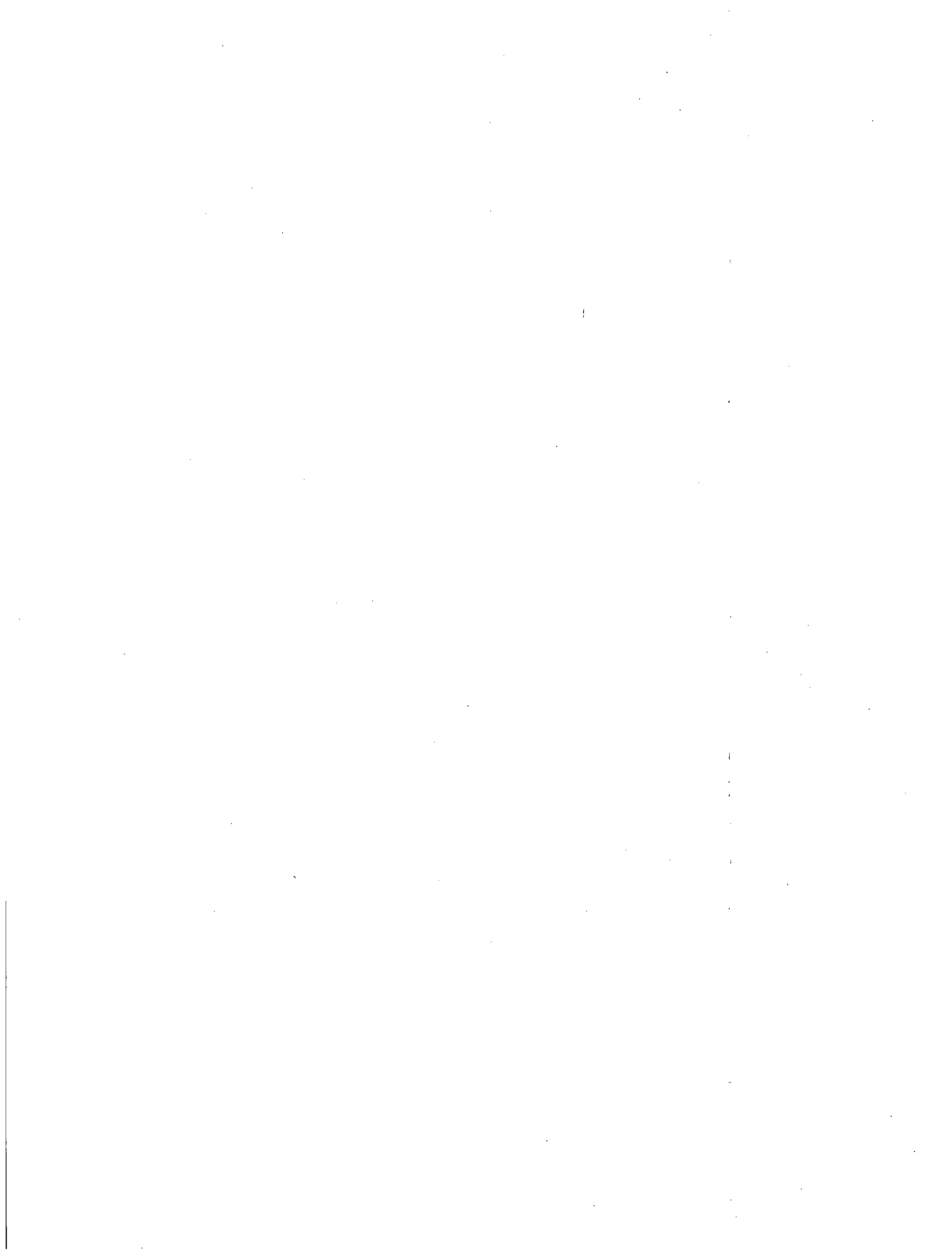
The NDE and DE on the North Anna 2 nozzles do not provide any meaningful information on the usefulness of TOFD and ET at detecting and characterizing flaws in a CRDM penetration tube. There were no significant flaws in the penetration tubes in any of the nozzles precluding an evaluation of these techniques. The evaluations of the penetration tubes did determine that the eddy current techniques can detect scratches and surface blemishes on the interiors of the penetration tubes, and that the TOFD and ultrasonic techniques appear to be able to detect fabrication flaws in the penetration tubes and welding flaws.

The ultrasonic leakage path measurements were partially successful. Nozzle 31 was accurately called as a leaking nozzle using the leakage path UT examination, and the ultrasonic fingerprint used to make the call was in fact based on physical characteristics caused by the leakage. The leakage path measurements did, however, miss one leakage path in Nozzle 31. Nozzle 54, which did not leak, was correctly called as a non-leaking nozzle by the UT leakage path measurements. There has been some interest in the nuclear industry to explore the development of leakage path measurements as a tool for ISI. Additional study would be required to make this a viable ISI tool, given the limited application of this technique and the mixed success.

## 9 Conclusions

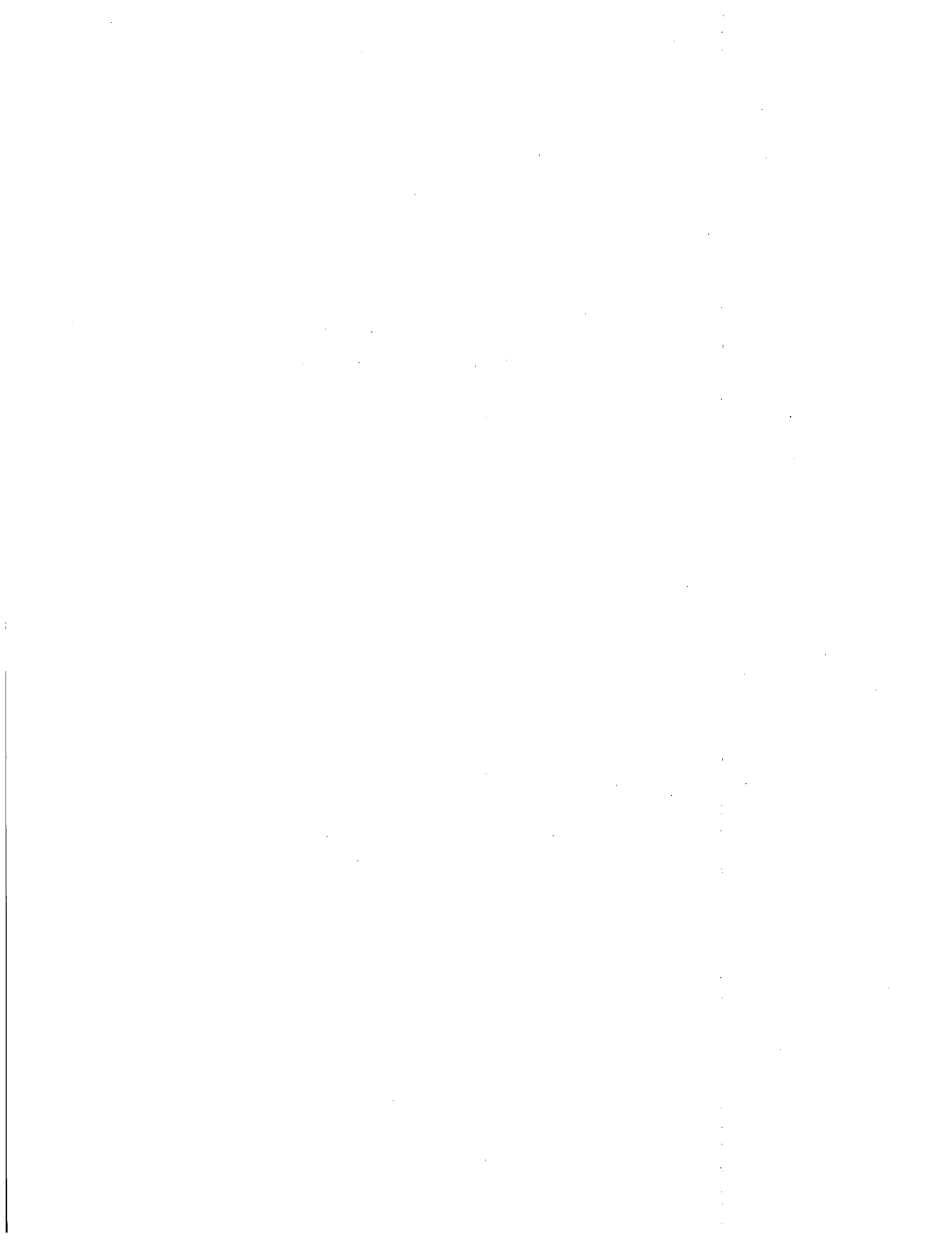
Industry vendors and PNNL applied conventional and state-of-the-art NDE techniques to Nozzles 31 and 51 that had been removed from the decommissioned North Anna Unit 2 RVH. Conventional NDE methods were used by industry vendors and Westinghouse on Nozzle 54 from the same RVH. The purpose of the NDE was to detect and characterize any indications. Destructive examination was then conducted on Nozzles 31 and 54 to validate the NDE results. Based on the results of these studies, the following conclusions may be drawn:

- Visual testing via replicant was ineffective at finding PWSCC, as the cracks were very tight and short, and the surface conditions were not conducive to an accurate visual test. It is possible that the replicate would have produced better results if the replicate had been examined using a scanning electron microscope.
- Visual testing via high-resolution photography was ineffective at finding most cracks, as the geometry prevented a complete inspection, the surface conditions were poor, and the cracks were both very short and very tight. A through-weld crack was not clearly visible on the wetted surface of the J-groove weld, even when placed in an optical microscope. Bare-metal VT was useful in characterizing the cracks found at 200 and 225 degrees in Nozzle 31.
- Volumetric inspection of the Nozzle 31 J-groove weld using zero-degree ultrasound of frequencies ranging from 5 MHz to 500 kHz found many fabrication flaws but was not able to detect the through-weld crack because the crack was axially oriented and presented almost no surface area to the ultrasonic beam.
- Penetrant testing was ineffective at finding a through-weld crack because the crack was too tight at the surface to allow the penetrant dye into the crack in sufficient amounts to produce a visible indication. Penetrant testing was useful in finding other cracks and in following up the visual testing via replicant.
- Eddy current testing was the most useful technique for finding PWSCC on the J-groove weld and showed much higher sensitivity than any of the other techniques. Eddy current testing was able to detect a through-weld crack, all cracks detected using PT and verified with VT, and others that were detectable only with ET. The PNNL and ISI ET results for Nozzle 31 were very consistent. All six flaws found to penetrate approximately 6 mm (0.25 in.) into the weld metal were detected by the PNNL and ISI ET tests. Several flaws were found in the buttering region of Nozzle 54 that were not found by the ISI ET testing. However, not enough information is available on these flaws to determine the length or COD of the flaws.
- It would be very useful for a volumetric technique, such as TOFD, to be developed and deployed on the J-groove weld to verify ET results. Currently, only ET provides good sensitivity for inspecting the J-groove weld metal, and ET is incapable of depth-sizing flaws.
- A detailed characterization of ET noise levels and ET responses to fabrication flaws in J-groove welds would be helpful in discriminating between the possibly small and low-voltage responses of service-induced PWSCC and innocuous indications.



## 10 References

- Buisine D, F Cattant, J Champredonde, C Pichon, C Benhamou, A Gelpi, and M Vaindirlis. 1993. "Stress Corrosion Cracking in the Vessel Closure Head Penetrations of French PWRs." In *Proceedings of the Sixth International Symposium on Environmental Degradation of Materials in Nuclear Power Systems – Water Reactors*, RE Gold and EP Simonen (eds), pp. 845–851. Minerals, Metals Materials Society, Warrendale, Pennsylvania.
- Champigny F, C Pages, and C Amzallag. 2002. "Vessel Head Penetrations: French Approaches for Maintenance in the PLIM Program." Presented to the *International Symposium on Nuclear Power Plant Life Management*, IAEA-CN-92/37, November 4–8, 2002, Budapest, Hungary.
- Doctor SR, GJ Schuster, and MT Anderson. 2004. "Primary Water Stress Corrosion Crack Morphology and Nondestructive Evaluation Reliability." Presented to the *4th International Conference on NDE in Relation to Structural Integrity for Nuclear and Pressurised Components*, December 6–8, 2004, London, United Kingdom.
- Ekström P and J Wåle. 1995. *Crack Characterization for In-service Inspection Planning*. SKI Report 95:70, Swedish Nuclear Power Inspectorate, Stockholm, Sweden.
- Embring G and EB Pers-Anderson. 1994. "Investigation of a Weld Defect, Reactor Vessel Head Ringhals" Presented to the *International Symposium on the Contribution of Materials Investigation to the Resolution of Problems in Pressurized Water Reactors*, September 12–16, 1994, Fontevraud, France.
- EPRI. 2005. *Materials Reliability Program: Destructive Examination of the North Anna 2 Reactor Pressure Vessel Head (MRP-142): Phase 1: Penetration Selection, Removal, Decontamination, Replication, and Nondestructive Examination*. Report 1007840, Electric Power Research Institute, Palo Alto, California.
- EPRI. 2006. *Materials Reliability Program: Destructive Examination of the North Anna 2 Reactor Pressure Vessel Head (MRP-198): Phase 3: A Comparison of Nondestructive and Destructive Examination Findings for CRDM Penetration #54*. Report 1013414, Electric Power Research Institute, Palo Alto, California.
- Faidy C, C Pichon, S Bhandaris, and J Vagner. 1994. "Stress Corrosion Cracking in French PWR CRDM Penetrations." Presented to *SISSI 94: Saclay International Seminar on Structural Integrity*, April 28–29, 1994, Saclay, France.
- Lang TA. 2003. "Significant Corrosion of the Davis-Besse Nuclear Reactor Pressure Vessel Head." In *ASME 2003 Pressure Vessels and Piping Conference (PVP2003)*, July 20–24, 2003, Cleveland, Ohio. American Society of Mechanical Engineers, New York.
- MacDonald DE. 1985. *IGSCC Detection in BWR Piping Using the MINAC*. EPRI-NP-3828, Electric Power Research Institute, Palo Alto, California.



**BIBLIOGRAPHIC DATA SHEET**

(See instructions on the reverse)

NUREG/CR-6996

2. TITLE AND SUBTITLE

Nondestructive and Destructive Examination Studies on Removed-from-Service Control Rod Drive Mechanism Penetrations

3. DATE REPORT PUBLISHED

MONTH	YEAR
July	2009

4. FIN OR GRANT NUMBER

Y6867

5. AUTHOR(S)

S.E. Cumblidge, S.R. Doctor, G.J. Schuster, R.V. Harris,  
S.L. Crawford, R.J. Seffens, M.B. Toloczko, S.M. Bruemmer

6. TYPE OF REPORT

Technical

7. PERIOD COVERED (Inclusive Dates)

8. PERFORMING ORGANIZATION - NAME AND ADDRESS (If NRC, provide Division, Office or Region, U.S. Nuclear Regulatory Commission, and mailing address; if contractor, provide name and mailing address.)

Pacific Northwest National Laboratory  
P.O. Box 999  
Richland, Washington 99352

9. SPONSORING ORGANIZATION - NAME AND ADDRESS (If NRC, type "Same as above"; if contractor, provide NRC Division, Office or Region, U.S. Nuclear Regulatory Commission, and mailing address.)

Division of Engineering  
Office of Nuclear Regulatory Research  
U.S. Nuclear Regulatory Commission  
Washington, DC 20555-0001

10. SUPPLEMENTARY NOTES

W. E. Norris, NRC Project Manager

11. ABSTRACT (200 words or less)

Control rod drive mechanism (CRDM) nozzles and J groove weldments were removed from the decommissioned North Anna Unit 2 reactor pressure vessel (RPV) head and shipped to Pacific Northwest National Laboratory (PNNL) in Richland, Washington, and Westinghouse Electric Company LLC in Pittsburgh, Pennsylvania, for study. The primary objectives of the research were to evaluate the effectiveness and reliability of nondestructive examination (NDE) methods as related to the in-service inspection of CRDM nozzles and J-groove weldments and to enhance the knowledge base of primary water stress corrosion cracking (PWSCC) through destructive characterization of the CRDM assemblies.

The first finding was that a significant number of the NDE indications were actually determined to be fabrication-related. The second finding was a realization that the meandering and branched nature of PWSCC can greatly affect detection and characterization. PWSCC cracks are generally tight at the surface. These findings provide a basis for explaining why it can be more difficult to detect cracks than leaks through in-service inspections.

12. KEY WORDS/DESCRIPTORS (List words or phrases that will assist researchers in locating the report.)

Control Rod Drive Mechanism, CRDM; Nozzle; Primary water stress corrosion cracking, PWSCC; Stress corrosion cracking, SCC; North Anna Unit 2; Nondestructive Evaluation, NDE; Ultrasonic testing, UT; Time of flight diffraction, TOFD; Eddy Current Testing, ET; Visual Testing, VT; Penetrant testing, PT; Nuclear Regulatory Commission, NRC; J-groove weld

13. AVAILABILITY STATEMENT

unlimited

14. SECURITY CLASSIFICATION

(This Page)

unclassified

(This Report)

unclassified

15. NUMBER OF PAGES

16. PRICE



Federal Recycling Program





UNITED STATES  
NUCLEAR REGULATORY COMMISSION  
WASHINGTON, DC 20555-0001

OFFICIAL BUSINESS